

High-Resolution Spectroscopic Measurements of the ν_5 Bending Vibration–Rotation Band of HCCN in its $\tilde{X}^3\Sigma^-$ State at 129 cm^{-1}

Michael D. Allen,^{*,1} Kenneth M. Evenson,^{*} and John M. Brown[†]

^{*}National Institute of Standards and Technology, Time and Frequency Division 847, 325 Broadway, Boulder, Colorado 80303; and [†]Physical and Theoretical Chemistry Laboratory, Oxford University, South Parks Road, Oxford OX1 3QZ, United Kingdom

Received July 14, 2000; in revised form June 4, 2001

The HCCN radical is known to be a quasi-linear molecule in its ground triplet state ($^3\Sigma^-$ in the linear configuration). Vibration–rotation transitions in the HCC bending (ν_5) fundamental band have been detected around 129 cm^{-1} by the technique of far-infrared laser magnetic resonance (FIR LMR). Four FIR laser lines were used to record a total of 530 resonances. The observed transitions can be regarded equivalently as $K_a = 1 \leftarrow 0$ transitions of a bent molecule or as $l_5 = 1 \leftarrow 0$ transitions of a linear molecule. The LMR data, combined with previous measurements on this molecule at microwave and submillimeter wavelengths, have been used to determine parameters of an asymmetric rotor Hamiltonian. The ν_5 band origin has been determined more accurately as $128.907\,968\,7(40)\text{ cm}^{-1}$. In addition, it has been possible to characterize the electron spin splittings in the $K_a = 1$ levels more reliably. Both ^1H and ^{14}N hyperfine splittings have been observed for the $K_a = 1$ levels for the first time; they show that the nuclear spin–electron spin dipolar interactions are markedly noncylindrical. Values for the electron spin and rotational g -factors ($g_s^{\alpha\alpha}$ and $g_r^{\alpha\alpha}$) have also been determined. © 2001 Academic Press

Key Words: FIR LMR; bending vibration–rotation transitions; quasilinear.

INTRODUCTION

The HCCN radical has been the subject of numerous investigations both experimentally (1–16) and theoretically (16–27). This is, in part, due to the initial disagreement between experiment and theory over the structure and geometry of the molecule. It has also been detected in the circumstellar envelope of the late-type carbon star IRC + 10216 and in the giant molecular clouds Sgr B2 and Orion A (28). The HCCN radical was first observed by Bernheim *et al.* (1–3). By measuring its EPR spectrum in a glassy solution at 77 K, they determined the electron spin–spin constants and concluded that the radical had a linear triplet ground state. Two early theoretical calculations by Hoffmann *et al.* (17) and Harrison *et al.* (18) supported the conclusion of a linear triplet ground state, but they were carried out with limited sized basis sets. All subsequent theoretical investigations, using larger basis sets and higher level of theory, have concluded that the HCCN radical has a bent triplet ground state with a low barrier to linearity (16,19–27). However, depending on the basis set and level of theory used there is still some controversy as to whether HCCN has a carbene ($\text{H}-\ddot{\text{C}}-\text{C}\equiv\text{N}$) or “allenic-like” ($\text{H}-\dot{\text{C}}=\text{C}=\dot{\text{N}}$) structure. In 1984 the ground state of HCCN was characterized by Saito *et al.* (8), who measured several low- J rotational transitions by microwave spectroscopy. They saw no deviation in the spectrum from the expectations for a linear molecule in a Σ state and so, in agreement with earlier experimental observations, they concluded that HCCN is a lin-

ear radical. A more thorough microwave study was conducted by Brown *et al.* (9), who measured the pure rotational spectrum of four isotopomers and were able to determine the substituted structure. They found an anomalously short internuclear distance (0.998 \AA) for the C–H separation and concluded, for the first time, that HCCN is quasi-linear instead of strictly linear. Further evidence for quasi-linearity came from an investigation of the ν_1 fundamental band by Morter *et al.* (10). They were able to observe hot bands associated with bending vibrations and, by intensity measurements, to estimate the energy for ν_5 at $187 \pm 20\text{ cm}^{-1}$, which indicates a very low barrier to linearity. A Fourier-transform microwave study was carried out by Endo and Ohshima (11). They were able to resolve the nuclear hyperfine structure, which suggested that the structure of HCCN was indeed “allene-like” and linear, with a large-amplitude CCH bending vibration. The evidence for quasi-linearity was further supported by McCarthy *et al.* (13), who made a millimeter-/submillimeter-wave measurement of pure rotational lines for both HCCN and DCCN in the ground and several excited vibrational levels. They fit their data using both asymmetric rotor model and linear models, the latter producing a much better fit of the data. Moreover, they were able to estimate the energies of the ν_5 levels by intensity measurements and reported a value of $145 \pm 15\text{ cm}^{-1}$ for the $1\nu_5^{\pm 1}$. This is considerably lower than the value, $187 \pm 20\text{ cm}^{-1}$, reported by the Curl group (10). Sun *et al.* (14) have recently reported measurements of the ν_1 and $\nu_1 + \nu_5$ bands of DCCN that permit an accurate determination of the ν_5 vibrational energy ($74.845 \pm 0.002\text{ cm}^{-1}$). A far-infrared laser magnetic resonance (FIR LMR) investigation of the ν_5 fundamental of DCCN, similar to this work, which will improve the

¹ National Research Council Postdoctoral Associate. Work supported by NASA contract W-19,167.

accuracy of the ν_5 separation (29), is under way. While the search for the ν_5 fundamental of HCCN was being conducted using FIR LMR (this work), the Curl group (15) reinvestigated the region around ν_1 and found the $\nu_1 + \nu_5$ band. This, combined with their earlier results on the $\nu_1 + \nu_5 - \nu_5$ band, provided an accurate determination of the ν_0 of the ν_5 vibrational fundamental band of HCCN ($128.907 \pm 0.002 \text{ cm}^{-1}$), which greatly simplified the search for the LMR spectrum.

This paper reports the first direct measurement of the ν_5 fundamental band (CCH bending vibrational mode in linear terms) of the HCCN radical. These measurements were made using FIR LMR spectroscopic techniques. From a quantum mechanical viewpoint, the data can be treated equivalently as either the $l = 1 \leftarrow 0$ transition of a linear molecule or as the $K_a = 1 \leftarrow 0$ transition of a bent molecule. We chose to use an asymmetric rotor Hamiltonian with the basis set truncated so that off-diagonal elements were restricted to the ranges $\Delta N = 4$ and $\Delta K_a = 0$. When the data are modeled in this fashion, the parameters determined can be related directly to those determined using a linear model for a polyatomic molecule. The data set included data from three sources. The first is the microwave data taken by Endo and Ohshima (11), in which hyperfine structure was resolved. The second is the millimeter-wave data recorded by McCarthy *et al.* (13) for the $\nu_5 = 0$ and 1 levels (30); hyperfine structure was not resolved in these observations. The third source is the FIR LMR data recorded for this work, in which hyperfine structure arising from both the ^1H nucleus ($I = 1/2$) and the ^{14}N nucleus ($I = 1$) was resolved in both the upper and lower states. With this complete set of data the molecular parameters were extended and refined. The LMR data taken in this work improves the accuracy of the value for the $\nu_5 = 1 \leftarrow 0$ separation and the spin-spin parameters and also determines hyperfine parameters for the upper state for the first time.

EXPERIMENTAL DETAILS

The far-infrared laser magnetic resonance spectrometer used for this work has been described in detail elsewhere (31). Two changes have been made recently which improve the sensitivity and short-wavelength performance of the spectrometer (32). The first change increased the Zeeman modulation frequency from 13 to 40 kHz, with a proportionate increase in sensitivity. The second change reduced the diameter of the tube, which constitutes the pump region of the LMR spectrometer, from 50.4 to 19 mm. Reducing the diameter of the tube increases the overlap of the FIR radiation field at short wavelengths with the pumped lasing gas. This increases the power of FIR laser lines below $100 \mu\text{m}$ and increases the number of lines lasing at these shorter wavelengths. These improvements are particularly important for the present experiment because all transitions observed for HCCN are at wavelengths well below $100 \mu\text{m}$. The signals were detected with a gallium-germanium photoconductor, processed by a lock-in amplifier at

$1 f$, and recorded with an xy plotter as a function of flux density. Since $1 f$ detection using magnetic modulation was employed, the signal is observed as the first derivative of an absorption profile.

The HCCN radical was produced using the method of hydrogen extraction by atomic fluorine, which has been proven effective in several previous investigations (33). The fluorine atoms were generated by flowing 10% F_2 in He through a microwave discharge. Acetonitrile (CH_3CN) and helium were added downstream, where the fluorine atoms removed two of the hydrogen atoms, resulting in the production of HCCN. A deep purple flame was observed when the production of HCCN was optimized. The helium introduced with the acetonitrile acted primarily as a carrier gas and pushed the reaction zone down into the laser beam, generating larger signals. The partial pressures of the gases at which optimal signals were obtained were 27 Pa (200 mTorr) 10% F_2 in He, 8 Pa (60 mTorr) acetonitrile, and 53 Pa (400 mTorr) He. Two checks were performed on most of the transitions to confirm that the signals were indeed due to HCCN. Either deuterated acetonitrile or methane replaced the regular acetonitrile. These checks eliminate or confirm species that contain hydrogen or nitrogen, respectively. In addition to these two tests, a third was performed on only a few lines. This test consisted of adding N_2 to the discharge with the F_2 in He mixture to produce N atoms, while adding methane downstream. This method proved effective in making HCCN, but not as efficient as the acetonitrile reaction.

Figure 1 shows a spectrum 60 mT wide observed for HCCN taken in perpendicular polarization ($\Delta M_J = \pm 1$) with a progression of M_J values for the $^Q Q_{22}(2)$ transition (notation $^{\Delta N} \Delta J_{F'F''}(N'')$). The sextet structure is due to the hyperfine splitting arising from the nuclear spin of the ^1H ($I = 1/2$) and ^{14}N ($I = 1$) nuclei. The doublet structure of the $M_J = 0 \leftarrow 1$ resonance shows the ^{14}N hyperfine structure collapsed while the hyperfine structure due to ^1H is still resolved. Figure 2 is a 50-mT-wide scan showing resonances associated with three different vibration-rotation transitions, $^P R_{13}(2)$, $^P Q_{23}(4)$, and $^P P_{11}(2)$, taken in parallel polarization ($\Delta M_J = 0$). Again, the sextet structure is due to hyperfine splitting arising from the ^1H and ^{14}N nuclei. The hyperfine structure in the $^P P_{11}(2)$ $M_J = 2$ resonance is somewhat unresolved. A simulated spectrum of the same region, generated using the parameters determined in this work, is included for comparison in both figures. The survey and measurement spectra were taken with the laser's electric field in both parallel ($E_\omega \parallel B_0$) and perpendicular ($E_\omega \perp B_0$) polarization to the magnetic field. Measurement scans were typically ≤ 10 mT in width, as shown in Fig. 3, and the resonances were recorded by tuning the magnet to the center of the line and waiting several time constants (100 ms) for the magnetic field to stabilize. The magnet was calibrated with an NMR gaussmeter. The overall experimental uncertainty is estimated to be $[(\pm 1 \times 10^{-4}) \times B \text{ (T)}]$ above 0.1 T and $\pm 1 \times 10^{-5}$ T below 0.1 T, where B is the magnetic flux density. The laser frequency is accurate to $[2^{1/2} \times (2 \times 10^{-7}) \times \nu_{\text{laser}}]$.

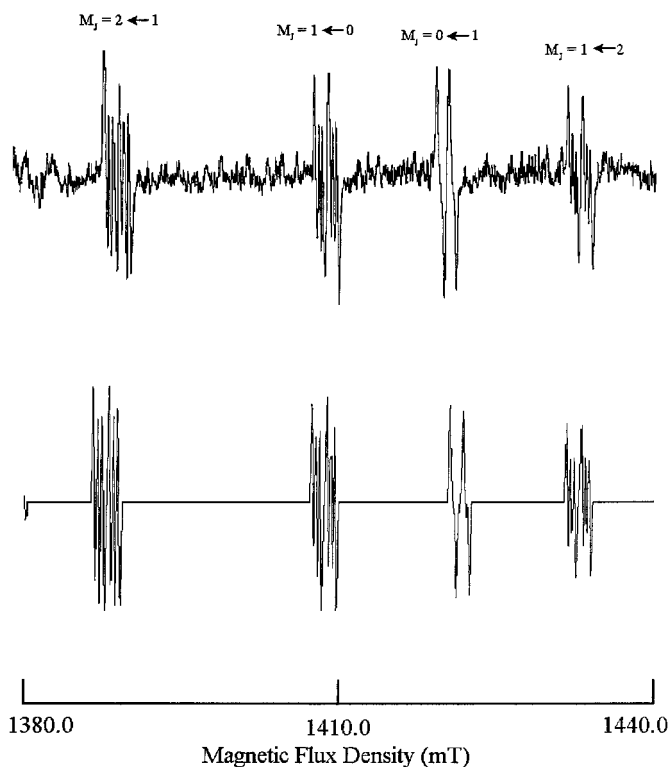
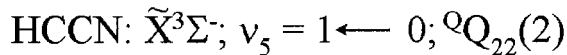


FIG. 1. Far-infrared laser magnetic resonance spectrum (upper trace) and simulated spectrum (lower trace) of the ν_5 ${}^Q Q_{22}(2)$ vibration–rotation transition of HCCN recorded in perpendicular polarization ($\Delta M_J = \pm 1$) covering 60 mT. The spectrum was recorded using the $77.905\text{-}\mu\text{m}$ (3 848 185.5-MHz) laser line of CH_3OH pumped by the 10R(16) line of a CO_2 laser. The sextet structure is due to the hyperfine splitting arising from the nuclear spin of the ${}^1\text{H}$ ($I = 1/2$) and the ${}^{14}\text{N}$ ($I = 1$) nuclei. The doublet structure of the $M_J = 0 \leftarrow 1$ resonance shows the ${}^{14}\text{N}$ hyperfine structure collapsed while the hyperfine structure due to ${}^1\text{H}$ is still resolved.

RESULTS AND ANALYSIS

Four far-infrared laser lines were used to record the LMR spectra reported in this paper. The details of these lines and the transitions recorded using each line are listed in Table 1. Figure 4 shows a stick diagram of the zero-field vibration–rotation transitions (frequencies given in Table 8), which were calculated using the molecular constants determined in this work and the positions of the four laser lines used in this study. A total of 530 resonances, corresponding to 45 different vibration–rotation transitions ranging in N'' from 0 to 9 and with $\Delta N = -1, 0$, and $+1$, were recorded and assigned. Four of these were observed on two different laser lines. However, the data set used in the least-squares fit contained only 367 resonances because the eigenstate identification routine in the fitting software was not able to pick up the correct eigenvalues for all of the resonances. This problem occurred when the Zeeman and hyperfine splittings from both

nuclei were included. These interactions split each J into $2J + 1$ M_J sub-levels and each M_J level into six M_I levels. Including these interactions, along with the fact that HCCN has relatively small values for the spin–spin and the spin–rotation constants, results in a high density of energy levels. As a result there are many level crossings and avoided level crossings that cause the routine to pick up the wrong eigenvalue. The complexity of the energy levels is illustrated in a tuning diagram in Fig. 5. Figure 5 shows one of the simplest transitions ($N = 1 \leftarrow 1$) with and without hyperfine splitting. The higher N transitions are too complicated to illustrate this point clearly. We found that the routine could then “pick up” the correct eigenvalue for the troublesome M_J levels if the eigenvalue identification took place at a field of 200 mT. At this low a field the levels have not tuned far enough to cross. In addition, hyperfine interaction was not included, which reduces the number of energy levels by a factor of 6. Therefore, several of the resonances in which hyperfine structure was resolved were

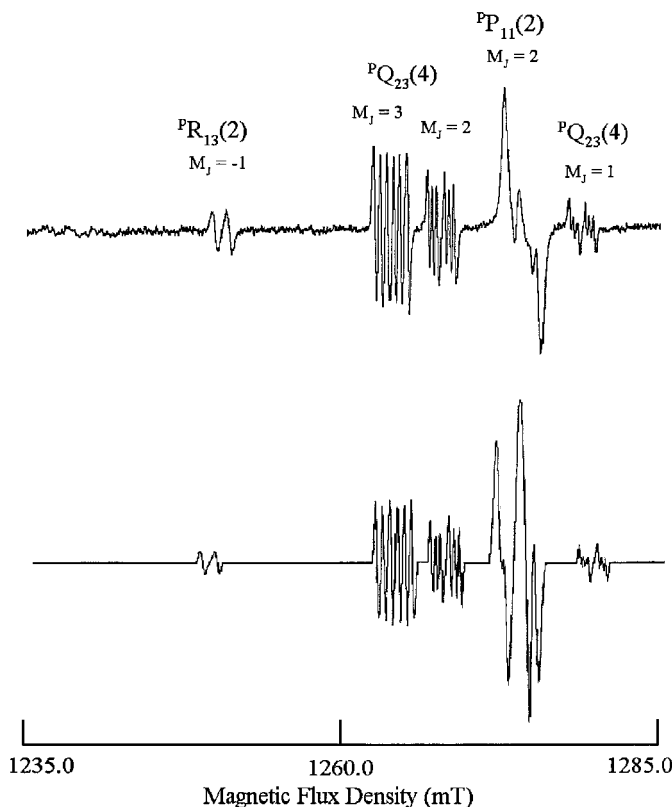
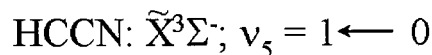


FIG. 2. Far-infrared laser magnetic resonance spectrum (upper trace) and simulated spectrum (lower trace) showing three different vibration–rotation transitions in the ν_5 bending fundamental of HCCN. This spectrum was recorded in parallel polarization ($\Delta M_J = 0$) covering 50 mT using the $77.905\text{-}\mu\text{m}$ (3 848 185.5-MHz) laser line of CH_3OH pumped by the 10R(16) line of a CO_2 laser. The sextet structure is due to the hyperfine splitting arising from the nuclear spin of the ${}^1\text{H}$ ($I = 1/2$) and the ${}^{14}\text{N}$ ($I = 1$) nuclei. The ${}^P R_{13}(2)$ and ${}^P P_{11}(2)$ transitions show unresolved hyperfine structure. The simulated spectrum is not perfect due to the large difference in tuning rates of the various vibration–rotation transitions.

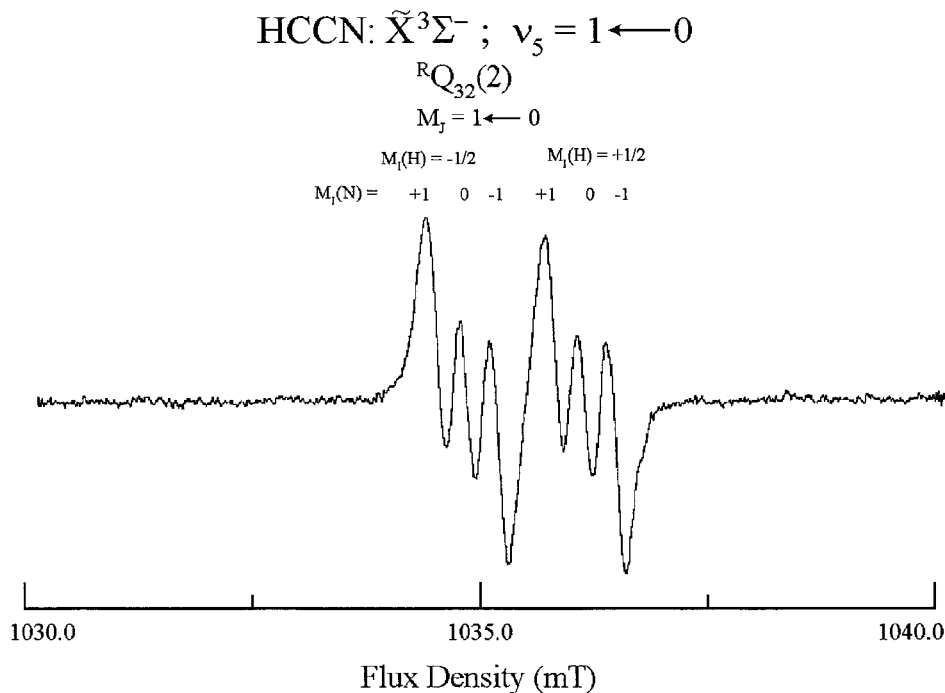


FIG. 3. Typical trace of a measurement scan showing the hyperfine structure due to the ^1H ($I = 1/2$) and the ^{14}N ($I = 1$) nuclei. This spectrum was recorded in perpendicular polarization ($\Delta M_J = \pm 1$) covering 10 mT using the 77.406 μm (3 873 005.1 MHz) laser line of CH_3OH pumped by the 9R(8) line of a CO_2 laser.

included in the fit neglecting hyperfine splitting (see Table 3). In these cases the resonant flux density was given the value of the average of the resolved hyperfine components. Hyperfine structure due to the ^1H nucleus was resolved and included in the fit for 71 of the 116 M_J components and for 49 of the 116 M_J components for the ^1H and the ^{14}N nuclei, respectively.

The initial FIR LMR search for the ν_5 fundamental band was made in the region predicted by McCarthy *et al.* (13), near 145 cm^{-1} . We were not able to make any assignments at that time. We then learned that the Curl group had reinvestigated the region near the ν_1 fundamental and observed the $\nu_1 + \nu_5$ combination band (15). The observation of this band along with their earlier work on the $\nu_1 + \nu_5 - \nu_5$ band (10) provided a much more accurate determination of the ν_5 separation, $128.907 \pm 0.002\text{ cm}^{-1}$. We used this value to make predictions and then conducted searches in the region indicated. From this, we were able to make assignments of the LMR observations.

We elected to use an effective Hamiltonian which described the energy levels of an asymmetric rotor in a nonsinglet electronic state to analyze the data, even though HCCN is thought to be a quasi-linear molecule and the pure rotational spectra have been shown to fit nicely using a linear model. This decision was made, in part, because we already had a computer program for an asymmetric rotor and only minor changes to the code were needed in order to fit the HCCN data. In addition, the $\nu_5 = 1 \leftarrow 0$ vibrational transition of a linear molecule has the same quantum mechanical representation as a $K_a = 1 \leftarrow 0$ rotational transition of a bent molecule. Consequently, the parameters determined using the asymmetric rotor model can be

related to those found for a linear molecule in its $\nu_5 = 0$ and 1 levels, as shown in Table 2.² The asymmetric rotor Hamiltonian used in this work is expressed in the N^2 formulation as the sum of several terms (33, 34):

$$\begin{aligned} H_{\text{eff}} = & H_{\text{rot}} + H_{\text{cd}} + H_{\text{ss}} + H_{\text{sscd}} + H_{\text{sr}} + H_{\text{srd}} \\ & + H_{\text{mhfs}} + H_{\text{Q}} + H_{\text{Zeem}}. \end{aligned} \quad [1]$$

Details of the individual terms H_{rot} , H_{cd} , H_{ss} , H_{sr} , H_{srd} , H_{mhfs} , and H_{Zeem} are given in Refs. (34, 35) and references within, so they will not be repeated here. Because HCCN behaves very much like a symmetric top from a rotational point of view, we have cast the centrifugal distortion corrections in H_{cd} and H_{srd} in the S-reduced form (36). The term H_{sscd} is not included in Refs. (34, 35). It describes the centrifugal distortion correction of the spin-spin interaction and is expressed as

$$\begin{aligned} H_{\text{sscd}} = & 1/2[(D_{\text{N}}^{\alpha} N^2 + D_{\text{K}}^{\alpha} N_z^2 + H_{\text{KN}}^{\alpha} N^2 N_z^2), \\ & (3S_z^2 - S^2)]_+ + \dots, \end{aligned} \quad [2]$$

where D_{N}^{α} , D_{K}^{α} , and H_{KN}^{α} describe the N^2 and K^2 dependence (centrifugal distortion) of the spin-spin coupling parameter

² The great majority of the linear molecule parameters in Table 2 are identical to those used by McCarthy *et al.* in their fit of the submillimeterwave data (13). The only exception is that we have chosen to use the l -type doubling parameters o_G , p_G , and q_G to describe the parity doubling whereas McCarthy *et al.* use the λ -type doubling parameters o , p , and q . As pointed out by Beaton and Brown (33), there is a difference of sign in the definitions of these two sets of parameters.

TABLE 1
FIR Laser Lines Used to Record LMR Spectra of the ν_5 Bending Fundamental of HCCN

CO ₂ Pump	Lasing Medium	Wavelength (μm)	Frequency (MHz)	HCCN Transitions observed		
				N_{KaKc}	$F'_i \leftarrow F''_i$ ^a	Linear Notation ^a
10R(20)	¹³ CD ₃ OD	73.467	4 080 637.2	10 ₁₁₀ \leftarrow 9 ₀₉	$F_1 \leftarrow F_1$	^R R ₁₁ (9)
				9R(8)	CH ₃ OH	77.406
1 ₁₀ \leftarrow 1 ₀₁	$F_1 \leftarrow F_1$ $F_2 \leftarrow F_3$ $F_3 \leftarrow F_2$	^Q S ₁₃ (1) ^Q R ₂₃ (1) ^Q P ₃₂ (1)				
				2 ₁₁ \leftarrow 2 ₀₂	$F_2 \leftarrow F_1$ $F_1 \leftarrow F_3$ $F_3 \leftarrow F_3$	^Q P ₂₁ (2) ^Q S ₁₃ (2) ^Q Q ₃₃ (2)
				3 ₁₂ \leftarrow 3 ₀₃	$F_1 \leftarrow F_1$ $F_3 \leftarrow F_3$	^Q Q ₁₁ (3) ^Q Q ₃₃ (3)
				4 ₁₃ \leftarrow 4 ₀₄	$F_3 \leftarrow F_3$	^Q Q ₃₃ (4)
				1 ₁₁ \leftarrow 0 ₀₀	$F_2 \leftarrow F_1$	^R Q ₂₁ (0)
				2 ₁₂ \leftarrow 1 ₀₁	$F_1 \leftarrow F_1$ $F_1 \leftarrow F_2$ $F_3 \leftarrow F_2$	^R R ₁₁ (1) ^R S ₁₂ (1) ^R Q ₃₂ (1)
				3 ₁₃ \leftarrow 2 ₀₂	$F_1 \leftarrow F_2$ $F_3 \leftarrow F_1$ $F_3 \leftarrow F_3$	^R S ₁₂ (2) ^R P ₃₁ (2) ^R Q ₃₂ (2)
				4 ₁₄ \leftarrow 3 ₀₃	$F_3 \leftarrow F_1$ $F_3 \leftarrow F_2$	^R P ₃₁ (3) ^R Q ₃₂ (3)
				5 ₁₅ \leftarrow 4 ₀₄	$F_3 \leftarrow F_2$	^R Q ₃₂ (4)
10R(16)	CH ₃ OH	77.904	3 848 185.5	1 ₁₁ \leftarrow 2 ₀₂	$F_1 \leftarrow F_1$ $F_1 \leftarrow F_3$ $F_3 \leftarrow F_3$	^P P ₁₁ (2) ^P R ₁₃ (2) ^P P ₃₃ (2)
				2 ₁₂ \leftarrow 3 ₀₃	$F_2 \leftarrow F_3$ $F_3 \leftarrow F_3$	^P Q ₂₃ (3) ^P P ₃₃ (3)
				3 ₁₃ \leftarrow 4 ₀₄	$F_2 \leftarrow F_3$	^P Q ₂₃ (4)
				4 ₁₄ \leftarrow 5 ₀₅	$F_2 \leftarrow F_3$	^P Q ₂₃ (5)
				1 ₁₀ \leftarrow 1 ₀₁	$F_1 \leftarrow F_1$ $F_2 \leftarrow F_1$ $F_1 \leftarrow F_2$ $F_3 \leftarrow F_2$	^Q Q ₁₁ (1) ^Q P ₂₁ (1) ^Q R ₁₂ (1) ^Q P ₃₂ (1)
				2 ₁₁ \leftarrow 2 ₀₂	$F_1 \leftarrow F_1$ $F_1 \leftarrow F_2$ $F_2 \leftarrow F_2$	^Q Q ₁₁ (2) ^Q R ₁₂ (2) ^Q Q ₂₂ (2)
				3 ₁₂ \leftarrow 3 ₀₃	$F_1 \leftarrow F_2$ $F_2 \leftarrow F_2$ $F_3 \leftarrow F_2$	^Q R ₁₂ (3) ^Q Q ₂₂ (3) ^Q P ₃₂ (3)
				4 ₁₃ \leftarrow 4 ₀₄	$F_1 \leftarrow F_2$ $F_3 \leftarrow F_2$	^Q R ₁₂ (4) ^Q P ₃₂ (4)
				5 ₁₄ \leftarrow 5 ₀₅	$F_1 \leftarrow F_2$ $F_3 \leftarrow F_2$	^Q R ₁₂ (5) ^Q P ₃₂ (5)
				6 ₁₅ \leftarrow 6 ₀₆	$F_1 \leftarrow F_2$ $F_3 \leftarrow F_2$	^Q R ₁₂ (6) ^Q P ₃₂ (6)
				7 ₁₆ \leftarrow 7 ₀₇	$F_1 \leftarrow F_2$	^Q R ₁₂ (7)
				1 ₁₁ \leftarrow 0 ₀₀	$F_2 \leftarrow F_1$	^R Q ₂₁ (0)
9R(8)	N ₂ H ₄	81.099	3 696 638.2	7 ₁₇ \leftarrow 8 ₀₈	$F_1 \leftarrow F_1$ $F_2 \leftarrow F_1$	^P P ₁₁ (8) ^P O ₂₁ (8)

^a F_i labels the spin components in order of increasing energy for a given J and linear notation given as $\Delta^N \Delta J_{F'_i F''_i}(N'')$.

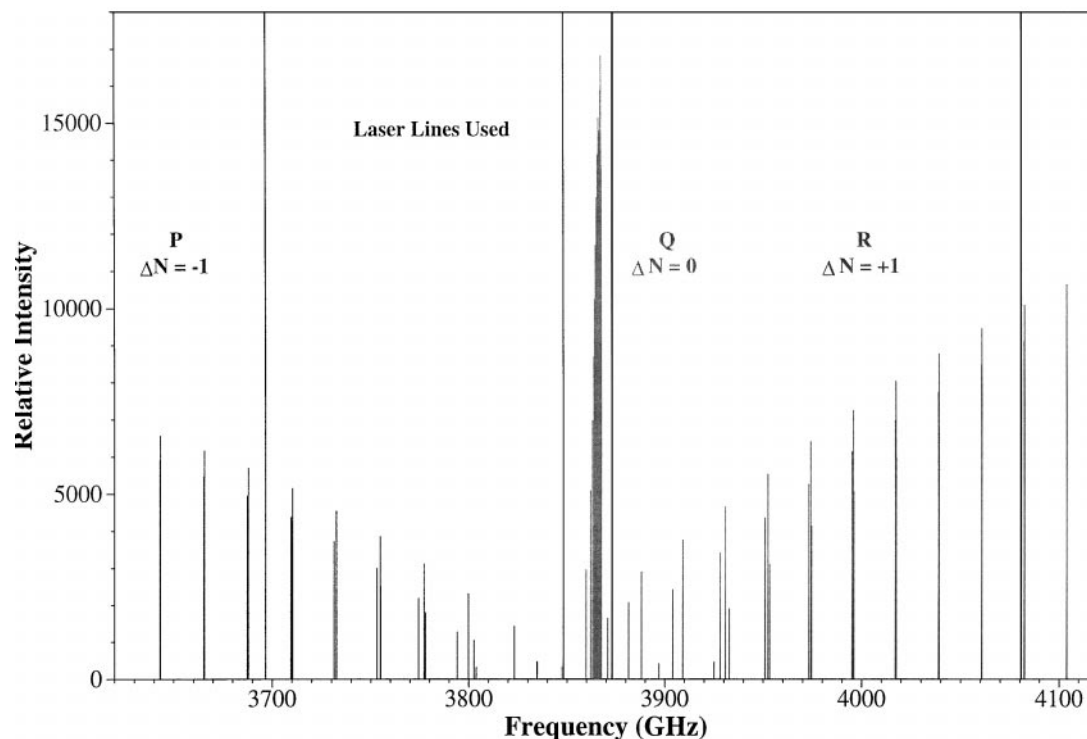


FIG. 4. Zero-field vibration-rotation transitions for the ν_5 bending fundamental calculated using the molecular constants determined in this work. The positions of the four laser lines (extended vertical lines) used in this study are also given. The transitions are all $\Delta J = \Delta N$ except the $N = 1 \leftarrow 0$.

(α). We included H_{sscd} because it was needed to make our Hamiltonian equivalent to that used by McCarthy *et al.* (13). As shown in Table 2, α , D_N^α , D_K^α , and H_{KN}^α in the bent molecule representation are related to the linear model's spin-spin terms, λ and λ_D , for the $\nu_5 = 0$ and 1 levels.

The effective Hamiltonian was used to analyze the data listed in Tables 3, 4, and 5. Table 3 reports the details of the FIR LMR data from this work. In addition to the LMR data we included the microwave data from Endo and Ohshima (11) in which hyperfine structure was resolved, listed in Table 4, and millimeter-wave data for the $\nu_5 = 0$ and 1 from McCarthy *et al.* (13, 30), given in Table 5.

Each observed resonance listed in Table 3 was initially given a weight equal to the inverse square of the estimated experimental uncertainty. The estimated experimental uncertainty of the FIR LMR data ranged from 1.5 to 4 MHz, based on the intensity of the resonance, the tuning rate, the uncertainty in the measurement of the magnetic flux density, and whether or not hyperfine structure was completely resolved. The resonances that were given uncertainties of 1.5 MHz were the strongest ones, in which the hyperfine structure was well resolved for either or both nuclei or completely collapsed, and the tuning rates were below 30.00 MHz/mT. All other resonances were given larger uncertainties because they were either not well resolved, weak, or observed at high field, had high tuning rates, or were in-

cluded without hyperfine because the software could not “pick up” the correct eigenvalue. The uncertainties seem appropriate since the standard deviation of the fit of 483 data points relative to the experimental uncertainty is 0.819. The microwave data and millimeter-wave data were given experimental uncertainties of 5 kHz and 50 kHz, respectively. After several attempted fits, 14 of the 367 resonances had residuals much greater than three times their uncertainty and, after reinvestigation of the spectra, they were subsequently given zero weight. The $N = 5 \leftarrow 4$ transition in the $K_a = 1$ ($\nu_5 = 1$) level of the millimeter-wave data was given zero weight because the residuals were abnormally large. This will be discussed in the next section.

The data set including all three types of data required 32 parameters, 29 varied and 3 fixed ($(bb)_Q$, g_N for ^1H , and g_N for ^{14}N), to model the data. The parameters determined in this fit are listed in Table 6 in units of both MHz and cm^{-1} . The parameters converted to linear molecule notation are given in Table 7 and compared with the best previously obtained values, where available. For the most part, the agreement is very good. The parameters determined include rotational parameters A , $1/2(B+C)$, $1/2(B-C)$, D_N , D_{NK} , d_1 , and H_{NK} , the spin-spin parameters α , β , D_N^α , D_K^α , and H_{KN}^α , the spin-rotation parameters ε_{aa} , $1/2(\varepsilon_{bb} + \varepsilon_{cc})$, $1/2(\varepsilon_{bb} - \varepsilon_{cc})$, $(D_{NK}^S + D_{KN}^S)$, D_{NK}^S , and D_N^S , the hyperfine parameters a_F , aa_1 , bb_1 (for both ^1H and ^{14}N), and aa_Q (for the ^{14}N

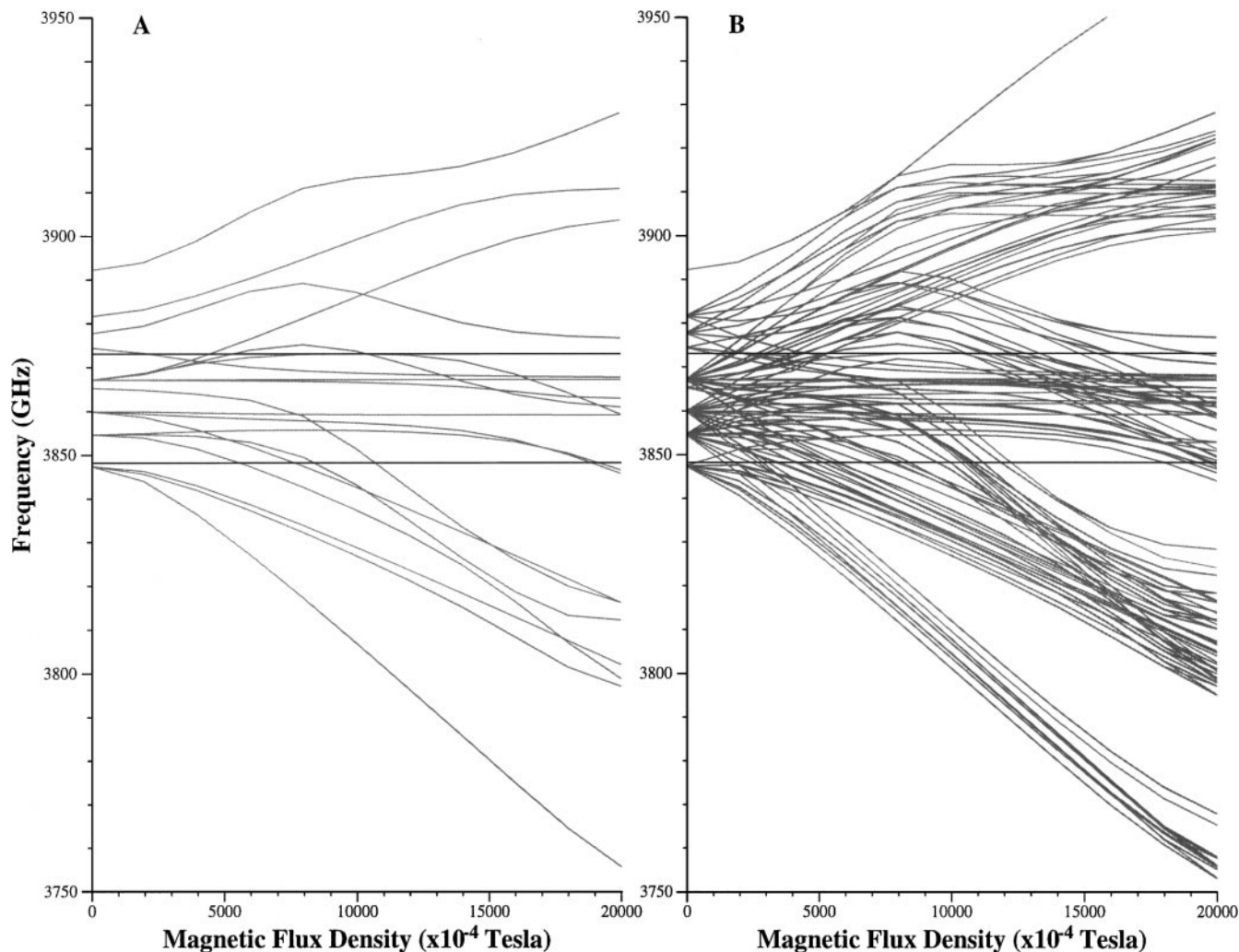


FIG. 5. Tuning diagram from 0 to 2 T (0 to 20 kG) for the $K_a = 1 \leftarrow 0$ ($v_5 = 1 \leftarrow 0$) $N = 1 \leftarrow 1$ transition in parallel polarization ($\Delta M_J = 0$). The diagram on the left (A) shows the transition exclusive of hyperfine splittings, while the diagram on the right (B) show the same transition with hyperfine splittings included. The high density of states on the right (B) shows the complexity of the transition and also explains why the eigenvalue pickup routine had difficulty in selecting the correct levels when hyperfine interactions were included.

nucleus), and the Zeeman parameters g_S^{aa} , $1/2(g_S^{bb} + g_S^{cc})$, g_r^{aa} , and $1/2(g_r^{bb} + g_r^{cc})$. The parameter $(bb)_Q$ was fixed at 0.974 MHz, which was obtained using the conversion $(bb)_Q = -1/2(aa)_Q$, that is, $(bb)_Q = (cc)_Q$. The values of g_N for the ^1H and ^{14}N nuclei were fixed to the nuclear magnetic moments for ^1H (5.58570) and ^{14}N (0.40376), respectively (37).

When the final fit was completed, we attempted another least-squares fit of the same data set with the basis set increased from $\Delta K_a = 0$ to $\Delta K_a = 2$. Had the molecule been truly bent then this test would have significantly improved the fit. However, increasing the basis set had very little effect on the fit, actually causing it to get slightly worse. There is therefore little support for a truly bent structure from the $K_a = 1 \leftarrow 0$ data.

DISCUSSION

We have detected vibration–rotation transitions in the v_5 fundamental band of the HCCN radical by FIR LMR spectroscopic techniques. These transitions fall into the FIR region because HCCN is quasi-linear due to the low barrier to linearity of the CCH bending vibration. This is the second measurement of a bending fundamental for carbon-chain species in a series of similar studies by the current authors using FIR LMR. The first was the measurement of the v_2 fundamental of the CCN radical (38). Previously, there had been two reports of bending fundamentals in the FIR region. One was for C_3 (39) and the other for FeD_2 (40).

TABLE 2
Parameter Conversion Relationships between Linear and Bent Models

Linear Notation	Bent Notation
ν_0 of ν_5	$(A - \bar{B}) - D_K$
B_0	$1/2(B + C)$
D_0	D_N
γ_0	$1/2(\epsilon_{bb} + \epsilon_{cc})$
γ_{D0}	D_N^S
λ_0	$3\alpha/2$
λ_{D0}	$3D_N^{\alpha}/2$
B_I	$1/2(B + C) - D_{NK} + H_{KN}$
D_I	$D_N - H_{NK}$
A_I	$\epsilon_{aa} - 1/2(\epsilon_{bb} + \epsilon_{cc}) - D_{NK}^S$
γ_I	$1/2(\epsilon_{bb} + \epsilon_{cc}) + (D_{NK}^S + D_{KN}^S)$
λ_I	$3\alpha/2 + 3D_K^{\alpha}/2$
λ_{DI}	$3D_N^{\alpha}/2 + 3H_{KN}^{\alpha}/2$
α_G	$-\beta$
p_G	$1/2(\epsilon_{bb} - \epsilon_{cc})$
q_G	$-1/2(B - C)$
q_{GD}	$-2d_1^a$
b_F (H)	a_F (H)
c (H)	$3aa_I$ (H)/2
b_F (N)	a_F (N)
c (N)	$3aa_I$ (N)/2
eQq_0 (N)	$aa_Q/2I(2I - 1)$ (N)

^a We have used Watson's S -reduction of the centrifugal distortion terms (36).

This study is a significant advance in our knowledge of the HCCN radical. It provides the most accurate determination of the ν_5 separation to date and a more reliable and accurate determination of the electron spin splittings. In addition, we have made the first observation of hyperfine structure in the $K_a = 1$ (or $\nu_5 = 1$) levels and a much more reliable and accurate determination of the spin and rotational g -factors. Twenty-nine parameters have been determined in the analysis, most of them significantly improved. The primary quantity determined in this work is the ν_5 vibrational interval; it can be calculated using the relationship in Table 2 as $\nu_5 = 128.907\,968\,7(40)\text{ cm}^{-1}$. It is more accurate than, but in excellent agreement with, the value determined by Han *et al.* (15), $128.907(2)\text{ cm}^{-1}$. The availability of this latter value considerably aided our analysis.

The present observations also provide a better determination of the spin splittings, particularly for the $K_a = 1$ levels, which had previously been studied only by McCarthy *et al.* (13) at submillimeter wavelengths. The latter's data are included in our fit. The data points all fitted very satisfactorily except for the $N = 5 \leftarrow 4$ frequencies at the $K_a = 1$ level (see Table 5). These five transitions could be fit much better if the parameter ϵ_{aa} was increased from -8.47 to -17.6 MHz, the value effectively used by McCarthy *et al.* in their fit (Tables 2 and 7). However,

McCarthy *et al.* detected only transitions with $\Delta J = \Delta N$ and so did not observe the spin splittings directly. In our work, on the other hand, we do obtain direct information on the spin splittings because we observe the $\Delta J \neq \Delta N$ transitions as well. Furthermore, the modeling of the Zeeman effect depends on the separations of the spin components. For these reasons, we believe our determination of the spin splittings is more reliable, although we do not have an explanation for the comparatively poor fit of the $N = 5 \leftarrow 4$ transition frequencies.

In the LMR study, we see proton and ^{14}N hyperfine splittings for HCCN at both $K_a = 0$ and 1 levels. Although the $K_a = 0$ had been well characterized previously by Endo and Ohshima (11), this is the first observation of the hyperfine splittings at the $K_a = 1$ levels. It is remarkable that we have been able to resolve such splittings with an experimental (Doppler) linewidth of 7.7 MHz (FWHM), whereas McCarthy *et al.*, with a narrower linewidth (about 0.6 MHz) were not. This result demonstrates one of the many merits of the LMR technique. In the submillimeter-wave study, which was made in the absence of a magnetic field, the nuclear spin is coupled to the rotational plus spin angular momentum, \mathbf{J} . The strong transitions are $\Delta F = \Delta F_1 = \Delta J = \Delta N = 1$ (see the footnote to Table 4 for an explanation of the quantum numbers). Since the hyperfine splittings do not change greatly with N , these transitions all occur at very similar frequencies and the hyperfine structure is not resolved. In the LMR experiment, on the other hand, the nuclear spins are decoupled from the molecular framework and the $\Delta M_1 = 0$ transitions usually connect states with different hyperfine splittings. The hyperfine structure is thus much more easily resolved. The observation of hyperfine splittings in the $K_a = 1$ levels provide an indication of the noncylindrical symmetry of the hyperfine interactions. The parameters in Table 6 show clearly that the dipole-dipole coupling for both ^1H and ^{14}N nuclei is distinctly non-cylindrical about the a -inertial axis. The ^{14}N electric quadrupole interaction, on the other hand, shows no deviation from cylindrical symmetry within experimental error.

The nuclear hyperfine parameters in Table 6 which govern the splittings in the $K_a = 0$ levels agree very well with those reported by Endo and Ohshima (11), although they are now better determined. This is not surprising, since we have included their transition frequencies in our fit (see Table 4). Endo and Ohshima give a thorough discussion of the structural implications of the hyperfine parameters and we shall not repeat it here. Suffice it to say that the parameters suggest that the electron spin ($S = 1$) is predominantly confined to the C_1 atom (adjacent to the H atom) and the N atom, 0.66 spin density on C_1 and 0.34 on N. This is consistent with a structure for HCCN that is two parts allenic and one part carbene.

The ^{14}N hyperfine parameters of HCCN make an interesting comparison with those of the related molecules CCN and NCN; the values available are collected in Table 8. Unfortunately, experimental values are not available for NCN but a high-level *ab initio* calculation of the magnetic hyperfine parameters has been carried out on this molecule (41). The parameters for

TABLE 3
Details of the ν_5 Bending Vibration–Rotation Transitions of HCCN Observed Using FIR LMR

$N' \leftarrow N''$	Parity ^a	$M_J' \leftarrow M_J''$	$M_1(^1\text{H})$	$M_1(^{14}\text{N})$	eigenstate id. # ^b	B_0 (mT)	$\nu_L - \nu_c$ (MHz)	$\partial\nu/\partial B_0$ (MHz/mT)	Uncert. (MHz)
<u>FIR Laser Frequency $\nu_L = 4080637.2$ MHz</u>									
10 \leftarrow 9	1	10 \leftarrow 10	1/2		1 \leftarrow 1	311.09	2.511	-10.15	3.0
		10 \leftarrow 10	-1/2		1 \leftarrow 1	309.20	-2.795	-10.14	3.0
<u>FIR Laser Frequency $\nu_L = 3873005.1$ MHz</u>									
1 \leftarrow 2	-1	0 \leftarrow 0			3 \leftarrow 1	1 870.60 ^c	-3.299	20.65	4.0
		2 \leftarrow 1			1 \leftarrow 1	1 124.16 ^c	1.104	23.75	4.0
1 \leftarrow 1	1	0 \leftarrow 0			1 \leftarrow 1	218.40	-1.365	-9.62	1.5
		-1 \leftarrow -1	1/2		2 \leftarrow 1	450.04	-1.807	21.22	1.5
		-1 \leftarrow -1	-1/2		2 \leftarrow 1	448.58	-1.631	21.21	1.5
		0 \leftarrow -1	1/2		3 \leftarrow 2	433.46	1.513	20.06	1.5
		0 \leftarrow -1	-1/2		3 \leftarrow 2	432.37	-0.064	20.07	1.5
		0 \leftarrow -1			3 \leftarrow 2	1 144.08 ^c	1.719	-19.07	4.0
2 \leftarrow 2	-1	1 \leftarrow 1			3 \leftarrow 2	89.33	-0.657	12.28	1.5
		1 \leftarrow 1	1/2	1	2 \leftarrow 1	208.98	2.461	20.69	1.5
		1 \leftarrow 1	1/2	0	2 \leftarrow 1	209.96	0.754	20.70	1.5
		1 \leftarrow 1	1/2	-1	2 \leftarrow 1	210.92	0.489	20.72	1.5
		1 \leftarrow 1	-1/2	1	2 \leftarrow 1	207.00	-0.244	20.67	1.5
		1 \leftarrow 1	-1/2	0	2 \leftarrow 1	207.89	-0.071	20.68	1.5
		1 \leftarrow 1	-1/2	-1	2 \leftarrow 1	208.98	-3.009	20.70	1.5
		1 \leftarrow 1			1 \leftarrow 1	847.37 ^c	2.217	17.19	4.0
		0 \leftarrow 0			3 \leftarrow 2	53.97	0.735	15.59	1.5
		0 \leftarrow 0	1/2		2 \leftarrow 1	312.49	0.188	19.78	1.5
		0 \leftarrow 0	-1/2		2 \leftarrow 1	311.20	0.350	19.78	1.5
		0 \leftarrow 0			1 \leftarrow 1	889.56 ^c	3.339	32.79	4.0
		-1 \leftarrow -1			3 \leftarrow 2	42.80	0.254	16.60	1.5
		-1 \leftarrow -1	1/2		2 \leftarrow 1	283.73	-0.766	19.38	1.5
		-1 \leftarrow -1	-1/2		2 \leftarrow 1	282.32	-0.831	19.38	1.5
		-2 \leftarrow -2			2 \leftarrow 1	42.80	-1.395	12.06	1.5
		0 \leftarrow -1			1 \leftarrow 1	890.59 ^c	-1.644	33.64	4.0
		0 \leftarrow -1			1 \leftarrow 1	933.68 ^c	0.474	22.06	4.0
3 \leftarrow 3	1	2 \leftarrow 2			1 \leftarrow 1	1 237.66 ^c	2.723	31.63	4.0
		1 \leftarrow 1			1 \leftarrow 1	1 246.34 ^c	2.207	34.93	4.0
		0 \leftarrow 0			1 \leftarrow 1	1 299.97 ^c	2.867	41.39	4.0
		4 \leftarrow 3	1/2		1 \leftarrow 1	502.78	-0.087	21.57	4.0
		4 \leftarrow 3	-1/2		1 \leftarrow 1	501.58	-5.716	21.58	0.0
		1 \leftarrow 2			1 \leftarrow 1	1 204.11 ^c	1.959	28.34	4.0
4 \leftarrow 4	-1	3 \leftarrow 3			1 \leftarrow 1	1 666.15 ^c	-1.863	40.21	4.0
		2 \leftarrow 2			1 \leftarrow 1	1 653.03 ^c	0.744	40.25	4.0
		1 \leftarrow 1			1 \leftarrow 1	1 669.91 ^c	-0.711	42.83	4.0
		0 \leftarrow 0			1 \leftarrow 1	1 699.38 ^c	-1.170	46.47	4.0
1 \leftarrow 0	-1	1 \leftarrow 1	1/2	1	1 \leftarrow 1	415.10	1.120	-22.93	1.5
		1 \leftarrow 1	1/2	0	1 \leftarrow 1	415.66	1.701	-22.92	1.5
		1 \leftarrow 1	1/2	-1	1 \leftarrow 1	416.05	-0.037	-22.92	1.5
		1 \leftarrow 1	-1/2	1	1 \leftarrow 1	413.47	0.636	-22.93	1.5
		1 \leftarrow 1	-1/2	0	1 \leftarrow 1	414.06	1.905	-22.93	1.5
		1 \leftarrow 1	-1/2	-1	1 \leftarrow 1	414.43	-0.292	-22.92	1.5
2 \leftarrow 1	1	0 \leftarrow 0	1/2	1	1 \leftarrow 3	690.32	-1.764	-35.42	1.5
		0 \leftarrow 0	1/2	0	1 \leftarrow 3	690.81	-1.082	-35.41	1.5
		0 \leftarrow 0	1/2	-1	1 \leftarrow 3	691.22	-1.536	-35.40	1.5
		0 \leftarrow 0	-1/2	1	1 \leftarrow 3	688.85	0.114	-35.42	1.5
		0 \leftarrow 0	-1/2	0	1 \leftarrow 3	689.34	0.794	-35.41	1.5
		0 \leftarrow 0	-1/2	-1	1 \leftarrow 3	689.74	-0.017	-35.41	1.5
		0 \leftarrow 0			2 \leftarrow 3	1 331.28 ^c	-0.381	-14.03	4.0
		-1 \leftarrow -1			1 \leftarrow 2	1 218.75 ^c	1.239	-23.47	4.0

^a Lower state parity; all transitions are electric dipole allowed. The parity is $-(-)^{K_c}$ for a molecule in a level $N_{K_a K_c}$ of a $^3A''$ state.

^b Eigenstate identification number labels the spin components in order of increasing energy for a given J .

^c Resonance observed with hyperfine structure resolved and eigenvalue identification took place at 200 mT.

TABLE 3—Continued

$N' \leftarrow N''$	Parity ^a	$M_J' \leftarrow M_J''$	M_1 (¹ H)	M_1 (¹⁴ N)	eigenstate id. # ^b	B_0 (mT)	$\nu_L - \nu_c$ (MHz)	$\partial\nu/\partial B_0$ (MHz/mT)	Uncert. (MHz)
		1 ← 2			1 ← 1	929.01 ^c	1.356	-17.01	4.0
		0 ← 1	1/2		2 ← 2	1 134.38	2.289	-19.41	1.5
		0 ← 1	-1/2		2 ← 2	1 132.92	-0.329	-19.43	1.5
		0 ← 1	1/2		1 ← 2	609.39	0.462	-41.84	1.5
		0 ← 1	-1/2		1 ← 2	608.23	1.533	-41.83	1.5
		1 ← 0	1/2	1	1 ← 3	717.16	1.438	-31.58	1.5
		1 ← 0	1/2	0	1 ← 3	717.64	1.608	-31.58	1.5
		1 ← 0	1/2	-1	1 ← 3	718.03	-0.793	-31.60	1.5
		1 ← 0	-1/2	1	1 ← 3	715.60	1.330	-31.57	1.5
		1 ← 0	-1/2	0	1 ← 3	716.08	1.496	-31.57	1.5
		1 ← 0	-1/2	-1	1 ← 3	716.54	1.303	-31.58	1.5
3 ← 2	-1	2 ← 2	1/2	1	1 ← 2	1 023.56	-0.420	-40.59	3.0
		2 ← 2	1/2	0	1 ← 2	1 023.89	-1.932	-40.61	3.0
		2 ← 2	1/2	-1	1 ← 2	1 024.29	-2.472	-40.62	3.0
		2 ← 2	-1/2	1	1 ← 2	1 022.07	-0.881	-40.58	3.0
		2 ← 2	-1/2	0	1 ← 2	1 022.41	-1.986	-40.59	3.0
		2 ← 2	-1/2	-1	1 ← 2	1 022.83	-1.714	-40.60	3.0
		0 ← 0	1/2	1	1 ← 3	1 032.39	-0.071	-45.47	3.0
		0 ← 0	1/2	0	1 ← 3	1 032.67	-0.594	-45.47	3.0
		0 ← 0	1/2	-1	1 ← 3	1 032.93	-1.898	-45.47	3.0
		0 ← 0	-1/2	1	1 ← 3	1 031.07	0.589	-45.47	3.0
		0 ← 0	-1/2	0	1 ← 3	1 031.35	0.067	-45.47	3.0
		0 ← 0	-1/2	-1	1 ← 3	1 031.58	-2.602	-45.47	3.0
		0 ← 0	1/2	1	2 ← 3	1 892.28	1.337	-23.63	3.0
		0 ← 0	1/2	0	2 ← 3	1 892.66	0.220	-23.62	3.0
		0 ← 0	1/2	-1	2 ← 3	1 892.98	-1.967	-23.62	3.0
		0 ← 0	-1/2	1	2 ← 3	1 890.71	-0.785	-23.64	3.0
		0 ← 0	-1/2	0	2 ← 3	1 891.14	-0.718	-23.63	3.0
		0 ← 0	-1/2	-1	2 ← 3	1 891.53	-1.249	-23.63	3.0
		-1 ← -1	1/2	1	1 ← 3	1 068.22	1.463	-48.90	3.0
		-1 ← -1	1/2	0	1 ← 3	1 068.66	1.442	-48.89	3.0
		-1 ← -1	1/2	-1	1 ← 3	1 069.05	1.640	-48.88	3.0
		-1 ← -1	-1/2	1	1 ← 3	1 066.73	0.913	-48.90	3.0
		-1 ← -1	-1/2	0	1 ← 3	1 067.16	0.401	-48.90	3.0
		-1 ← -1	-1/2	-1	1 ← 3	1 067.54	0.109	-48.89	3.0
		-2 ← -2	1/2		1 ← 2	1 898.76	0.835	-26.04	3.0
		-2 ← -2	-1/2		1 ← 2	1 897.36	0.887	-26.04	3.0
		2 ← 3			1 ← 1	1 220.24 ^c	0.922	-17.65	4.0
		1 ← 2	1/2	1	1 ← 2	1 056.84	-0.370	-38.15	3.0
		1 ← 2	1/2	0	1 ← 2	1 057.17	0.378	-38.16	3.0
3 ← 2	-1	1 ← 2	1/2	-1	1 ← 2	1 057.45	-1.004	-38.16	3.0
		1 ← 2	-1/2	1	1 ← 2	1 055.50	0.689	-38.14	3.0
		1 ← 2	-1/2	0	1 ← 2	1 055.85	2.200	-38.14	3.0
		1 ← 2	-1/2	-1	1 ← 2	1 056.15	1.580	-38.15	3.0
		0 ← 1			1 ← 3	1 017.62 ^c	-2.416	-46.35	4.0
		1 ← 0	1/2	1	1 ← 3	1 034.97	1.371	-40.93	3.0
		1 ← 0	1/2	0	1 ← 3	1 035.23	-1.870	-40.94	3.0
		1 ← 0	1/2	-1	1 ← 3	1 035.60	-1.044	-40.94	3.0
		1 ← 0	-1/2	1	1 ← 3	1 033.57	1.575	-40.92	3.0
		1 ← 0	-1/2	0	1 ← 3	1 033.90	1.198	-40.93	3.0
		1 ← 0	-1/2	-1	1 ← 3	1 034.23	0.386	-40.93	3.0
4 ← 3	1	3 ← 3	1/2	1	1 ← 2	1 410.24	-1.592	-45.65	3.0
		3 ← 3	1/2	0	1 ← 2	1 410.72	-1.739	-45.65	3.0
		3 ← 3	1/2	-1	1 ← 2	1 411.25	-1.155	-45.66	3.0
		3 ← 3	-1/2	1	1 ← 2	1 408.68	0.721	-45.64	3.0
		3 ← 3	-1/2	0	1 ← 2	1 409.14	-0.340	-45.65	3.0
		3 ← 3	-1/2	-1	1 ← 2	1 409.65	-0.670	-45.65	3.0
		2 ← 2	1/2	1	1 ← 3	1 401.80	-3.212	-45.36	3.0
		2 ← 2	1/2	0	1 ← 3	1 402.12	-4.095	-45.36	3.0
		2 ← 2	1/2	-1	1 ← 3	1 402.50	-3.648	-45.37	3.0

TABLE 3—Continued

$N' \leftarrow N''$	Parity a	$M_j' \leftarrow M_j''$	$M_1 (^1\text{H})$	$M_1 (^{14}\text{N})$	eigenstate id. # b	B_0 (mT)	$\nu_L - \nu_c$ (MHz)	$\partial\nu/\partial B_0$ (MHz/mT)	Uncert. (MHz)
		1 ← 1	-1/2	1	2 ← 1	609.82	-1.258	33.68	1.5
		1 ← 1	-1/2	0	2 ← 1	610.53	-1.244	33.67	1.5
		1 ← 1	-1/2	-1	2 ← 1	611.24	-1.115	33.67	1.5
		1 ← 1			2 ← 1	1 369.39 ^c	-3.067	-29.70	4.0
		0 ← 0	1/2	1	3 ← 1	505.71	-0.071	40.81	1.5
		0 ← 0	1/2	0	3 ← 1	506.10	0.692	40.81	1.5
		0 ← 0	1/2	-1	3 ← 1	506.50	0.702	40.81	1.5
		0 ← 0	-1/2	1	3 ← 1	504.25	-2.059	40.82	1.5
		0 ← 0	-1/2	0	3 ← 1	504.65	-1.713	40.82	1.5
		0 ← 0	-1/2	-1	3 ← 1	505.02	-0.487	40.81	1.5
		-1 ← -1	1/2		2 ← 1	1 249.25	1.421	23.35	4.0
		-1 ← -1	-1/2		2 ← 1	1 248.16	2.368	23.34	4.0
		1 ← 0	1/2	1	2 ← 1	645.10	0.116	37.05	1.5
		1 ← 0	1/2	0	2 ← 1	645.50	-0.041	37.06	1.5
		1 ← 0	1/2	-1	2 ← 1	645.86	-0.597	37.07	1.5
1 ← 2	-1	1 ← 0	-1/2	1	2 ← 1	643.63	0.935	37.05	1.5
		1 ← 0	-1/2	0	2 ← 1	643.98	2.628	37.05	1.5
		1 ← 0	-1/2	-1	2 ← 1	644.37	0.959	37.06	1.5
		0 ← -1	1/2		2 ← 1	1 020.27	-1.755	24.99	1.5
		0 ← -1	-1/2		2 ← 1	1 019.03	0.153	24.98	1.5
2 ← 3	1	2 ← 2	1/2	1	2 ← 1	875.59	2.718	47.36	1.5
		2 ← 2	1/2	0	2 ← 1	876.06	1.861	47.36	1.5
		2 ← 2	1/2	-1	2 ← 1	876.55	2.650	47.36	1.5
		2 ← 2	-1/2	1	2 ← 1	874.12	-1.631	47.36	1.5
		2 ← 2	-1/2	0	2 ← 1	874.55	-0.585	47.36	1.5
		2 ← 2	-1/2	-1	2 ← 1	875.06	-0.736	47.36	1.5
		1 ← 1			2 ← 1	1 758.76 ^c	0.364	30.49	4.0
		1 ← 1			3 ← 1	895.25 ^c	10.453	47.36	0.0
		0 ← 0			2 ← 1	1 618.86 ^c	0.221	47.09	4.0
3 ← 4	-1	3 ← 3	1/2	1	2 ← 1	1 262.36	0.824	50.91	3.0
		3 ← 3	1/2	0	2 ← 1	1 262.85	1.778	50.91	3.0
		3 ← 3	1/2	-1	2 ← 1	1 263.40	1.792	50.91	3.0
		3 ← 3	-1/2	1	2 ← 1	1 260.78	-1.429	50.91	3.0
		3 ← 3	-1/2	0	2 ← 1	1 261.27	-0.470	50.91	3.0
		3 ← 3	-1/2	-1	2 ← 1	1 261.82	-0.453	50.91	3.0
		2 ← 2	1/2	1	3 ← 1	1 266.31	1.693	50.58	3.0
		2 ← 2	1/2	0	3 ← 1	1 266.66	2.510	50.58	3.0
		2 ← 2	1/2	-1	3 ← 1	1 267.07	1.610	50.58	3.0
		2 ← 2	-1/2	1	3 ← 1	1 264.92	-0.923	50.58	3.0
		2 ← 2	-1/2	0	3 ← 1	1 265.29	-1.115	50.58	3.0
		2 ← 2	-1/2	-1	3 ← 1	1 265.67	-0.495	50.58	3.0
		1 ← 1	1/2	1	3 ← 1	1 277.21	1.988	51.28	3.0
		1 ← 1	1/2	0	3 ← 1	1 277.54	0.128	51.28	3.0
		1 ← 1	1/2	-1	3 ← 1	1 277.86	-0.864	51.28	3.0
		1 ← 1	-1/2	1	3 ← 1	1 275.93	-0.178	51.45	3.0
		1 ← 1	-1/2	0	3 ← 1	1 276.20	1.343	51.54	3.0
		1 ← 1	-1/2	-1	3 ← 1	1 276.48	2.834	51.66	3.0
4 ← 5	1	4 ← 4	1/2	1	2 ← 1	1 660.02	2.091	52.83	4.0
		4 ← 4	1/2	0	2 ← 1	1 660.57	2.268	52.83	4.0
		4 ← 4	1/2	-1	2 ← 1	1 661.15	2.614	52.83	4.0
		4 ← 4	-1/2	1	2 ← 1	1 658.45	-3.465	52.83	4.0
		4 ← 4	-1/2	0	2 ← 1	1 658.96	-1.174	52.83	4.0
		4 ← 4	-1/2	-1	2 ← 1	1 659.54	-0.824	52.83	4.0
		3 ← 3	1/2	1	3 ← 1	1 657.59	0.416	52.39	4.0
		3 ← 3	1/2	0	3 ← 1	1 657.98	1.643	52.40	4.0
		3 ← 3	1/2	-1	3 ← 1	1 658.45	0.028	52.40	4.0
		3 ← 3	-1/2	1	3 ← 1	1 656.17	-3.769	52.39	4.0
		3 ← 3	-1/2	0	3 ← 1	1 656.58	-3.589	52.39	4.0
		3 ← 3	-1/2	-1	3 ← 1	1 657.00	-2.582	52.39	4.0
		2 ← 2	1/2	1	3 ← 1	1 661.79	-1.185	52.58	4.0

TABLE 3—Continued

$N' \leftarrow N''$	Parity ^a	$M_J' \leftarrow M_J''$	M_1 (¹ H)	M_1 (¹⁴ N)	eigenstate id. # ^b	B_0 (mT)	$\nu_L - \nu_c$ (MHz)	$\partial\nu/\partial B_0$ (MHz/mT)	Uncert. (MHz)
1 ← 1	1	2 ← 2	1/2	0	3 ← 1	1 662.07	0.958	52.59	4.0
		2 ← 2	1/2	-1	3 ← 1	1 662.41	0.821	52.59	4.0
		1 ← 1			1 ← 1	1 892.76 ^c	0.755	-21.57	4.0
		1 ← 1			2 ← 2	850.60 ^c	-2.526	-28.49	4.0
		0 ← 0	1/2	1	1 ← 2	769.50	-8.916	-23.26	0.0
		0 ← 0	1/2	0	1 ← 2	770.23	-4.000	-23.26	1.5
		0 ← 0	1/2	-1	1 ← 2	770.87	-3.335	-23.27	1.5
		0 ← 0	-1/2	1	1 ← 2	768.32	1.933	-23.26	1.5
		0 ← 0	-1/2	0	1 ← 2	768.77	0.337	-23.26	1.5
		0 ← 0	-1/2	-1	1 ← 2	769.50	3.095	-23.27	0.0
		0 ← 0			3 ← 3	1 071.64 ^c	-3.148	-45.45	4.0
		-1 ← -1			2 ← 2	1 922.33 ^c	-2.721	-19.83	4.0
		1 ← 2			2 ← 1	1 088.76 ^c	0.432	-40.42	4.0
		0 ← 1			3 ← 2	996.05 ^c	1.468	-43.69	4.0
2 ← 2	-1	2 ← 2	1/2	1	1 ← 2	528.78	-1.166	-20.73	1.5
		2 ← 2	-1/2	0	1 ← 2	527.57	-1.269	-20.75	1.5
		2 ← 2			2 ← 2	1 427.29 ^c	-2.168	-44.52	4.0
		1 ← 1	1/2	1	1 ← 3	222.14	0.283	-40.74	1.5
		1 ← 1	1/2	0	1 ← 3	222.40	-0.565	-40.65	1.5
		1 ← 1	1/2	-1	1 ← 3	222.73	-0.680	-40.25	1.5
		1 ← 1	-1/2	1	1 ← 3	220.76	-1.704	-41.05	1.5
		1 ← 1	-1/2	0	1 ← 3	221.09	0.189	-41.04	1.5
		1 ← 1	-1/2	-1	1 ← 3	221.44	0.283	-41.07	1.5
		0 ← 0			1 ← 3	225.07 ^c	1.082	-39.85	4.0
		0 ← 0			3 ← 3	1 431.44 ^c	-1.624	-50.58	4.0
		-1 ← -1	1/2	1	1 ← 2	756.63	-1.883	-26.62	3.0
		-1 ← -1	1/2	0	1 ← 2	757.08	-2.445	-26.63	3.0
		-1 ← -1	1/2	-1	1 ← 2	757.59	-1.509	-26.64	3.0
		-1 ← -1	-1/2	1	1 ← 2	755.24	2.963	-26.61	3.0
		-1 ← -1	-1/2	0	1 ← 2	755.69	2.401	-26.62	3.0
		-1 ← -1	-1/2	-1	1 ← 2	756.15	2.005	-26.63	3.0
		-1 ← -1	1/2	1	1 ← 3	229.08	-1.787	-36.26	1.5
		-1 ← -1	1/2	0	1 ← 3	229.53	-1.562	-36.27	1.5
		-1 ← -1	1/2	-1	1 ← 3	229.93	-1.534	-36.28	1.5
		-1 ← -1	-1/2	1	1 ← 3	227.64	0.274	-36.25	1.5
		-1 ← -1	-1/2	0	1 ← 3	228.08	0.132	-36.26	1.5
		-1 ← -1	-1/2	-1	1 ← 3	228.51	1.245	-36.27	1.5
		1 ← 2			3 ← 2	1 431.70 ^c	3.207	-47.47	4.0
2 ← 1			2 ← 3	1 387.36 ^c	0.274	-44.50	4.0		
0 ← 1			3 ← 3	1 418.85 ^c	-0.667	-50.13	4.0		
3 ← 3	1	1 ← 0			3 ← 3	1 407.38 ^c	0.053	-47.67	4.0
		3 ← 3	1/2	1	1 ← 2	642.28	-2.210	-21.64	1.5
		3 ← 3	-1/2	0	1 ← 2	641.01	-2.097	-21.65	1.5
		3 ← 3			2 ← 2	1 835.47 ^c	1.521	-50.28	4.0
		2 ← 2			3 ← 3	1 809.27 ^c	-0.595	-50.77	4.0
		2 ← 2	1/2	1	1 ← 3	158.27	-0.739	-37.65	1.5
		2 ← 2	1/2	0	1 ← 3	158.64	-1.867	-37.66	1.5
		2 ← 2	1/2	-1	1 ← 3	159.14	-0.186	-37.67	1.5
3 ← 3	1	2 ← 2	-1/2	1	1 ← 3	156.83	0.570	-37.64	1.5
		2 ← 2	-1/2	0	1 ← 3	157.26	1.702	-37.65	1.5
		2 ← 2	-1/2	-1	1 ← 3	157.73	2.252	-37.67	1.5
		1 ← 1	1/2	1	1 ← 3	183.92	0.731	-38.28	1.5
		1 ← 1	1/2	0	1 ← 3	184.21	-0.828	-38.28	1.5
		1 ← 1	1/2	-1	1 ← 3	184.54	-1.502	-38.31	1.5
		1 ← 1	-1/2	1	1 ← 3	182.54	1.622	-38.27	1.5
		1 ← 1	-1/2	0	1 ← 3	182.84	0.438	-38.27	1.5
		1 ← 1	-1/2	-1	1 ← 3	183.17	-0.219	-38.30	1.5
		0 ← 0	1/2	1	1 ← 3	205.45	1.113	-39.06	1.5
		0 ← 0	1/2	0	1 ← 3	205.69	-0.651	-39.06	1.5
		0 ← 0	1/2	-1	1 ← 3	205.95	-1.755	-39.05	1.5

TABLE 3—Continued

$N' \leftarrow N''$	Parity ^a	$M_J' \leftarrow M_J''$	M_I (¹ H)	M_I (¹⁴ N)	eigenstate id. # ^b	B_0 (mT)	$\nu_L - \nu_c$ (MHz)	$\partial\nu/\partial B_0$ (MHz/mT)	Uncert. (MHz)
		0 ← 0	-1/2	1	1 ← 3	204.09	0.639	-39.06	1.5
		0 ← 0	-1/2	0	1 ← 3	204.43	2.780	-39.07	1.5
		0 ← 0	-1/2	-1	1 ← 3	204.71	2.457	-39.07	1.5
		-1 ← -1	1/2	1	1 ← 3	209.24	0.001	-36.55	1.5
		-1 ← -1	1/2	0	1 ← 3	209.61	0.304	-36.56	1.5
		-1 ← -1	1/2	-1	1 ← 3	209.95	0.289	-36.57	1.5
		-1 ← -1	-1/2	1	1 ← 3	207.80	-1.105	-36.54	1.5
		-1 ← -1	-1/2	0	1 ← 3	208.20	0.291	-36.56	1.5
		-1 ← -1	-1/2	-1	1 ← 3	208.57	1.369	-36.57	1.5
4 ← 4	-1	4 ← 4	1/2		1 ← 2	723.89	-2.374	-22.53	3.0
		4 ← 4	-1/2		1 ← 2	722.52	-2.730	-22.54	3.0
		3 ← 3	1/2	1	1 ← 3	138.96	3.377	-35.97	1.5
		3 ← 3	1/2	0	1 ← 3	139.39	2.008	-35.99	1.5
		3 ← 3	1/2	-1	1 ← 3	139.89	1.402	-36.01	1.5
		3 ← 3	-1/2	1	1 ← 3	137.25	-2.758	-35.95	1.5
		3 ← 3	-1/2	0	1 ← 3	137.74	-1.970	-35.97	1.5
		3 ← 3	-1/2	-1	1 ← 3	138.24	-2.584	-35.99	1.5
		3 ← 3	1/2		2 ← 3	513.24	1.090	-21.46	1.5
		3 ← 3	-1/2		2 ← 3	512.07	0.588	-21.48	1.5
		2 ← 2	1/2		2 ← 3	395.31	-0.137	-21.98	1.5
		2 ← 2	-1/2		2 ← 3	394.18	0.145	-21.99	1.5
		1 ← 1	1/2	1	1 ← 3	179.91	0.479	-36.44	1.5
		1 ← 1	1/2	0	1 ← 3	180.18	-1.403	-36.44	1.5
		1 ← 1	1/2	-1	1 ← 3	180.49	-1.965	-36.47	1.5
		1 ← 1	-1/2	1	1 ← 3	178.53	1.194	-36.43	1.5
		1 ← 1	-1/2	0	1 ← 3	178.87	1.850	-36.43	1.5
		1 ← 1	-1/2	-1	1 ← 3	179.21	2.412	-36.47	1.5
5 ← 5	1	5 ← 5	1/2		1 ← 2	786.01	0.556	-23.31	4.0
		5 ← 5	-1/2		1 ← 2	784.45	-2.669	-23.32	4.0
		4 ← 4	1/2	1	1 ← 3	136.25	-0.894	-35.31	1.5
		4 ← 4	1/2	0	1 ← 3	136.74	-1.382	-35.32	1.5
		4 ← 4	1/2	-1	1 ← 3	137.30	-0.914	-35.34	0.0
		4 ← 4	-1/2	1	1 ← 3	134.70	0.189	-35.30	1.5
		4 ← 4	-1/2	0	1 ← 3	135.21	0.406	-35.31	1.5
		4 ← 4	-1/2	-1	1 ← 3	135.77	0.868	-35.33	1.5
		4 ← 4	1/2		2 ← 3	582.71	-0.956	-21.77	1.5
5 ← 5	1	4 ← 4	-1/2		2 ← 3	581.54	-0.475	-21.78	1.5
		2 ← 2	1/2	1	1 ← 3	166.69	-1.710	-35.49	1.5
		2 ← 2	1/2	0	1 ← 3	167.03	-2.549	-35.51	1.5
		2 ← 2	1/2	-1	1 ← 3	167.41	-2.861	-35.53	1.5
		2 ← 2	-1/2	1	1 ← 3	165.34	2.068	-35.48	1.5
		2 ← 2	-1/2	0	1 ← 3	165.64	-0.181	-35.50	1.5
		2 ← 2	-1/2	-1	1 ← 3	166.05	0.577	-35.52	1.5
		1 ← 1	1/2	1	1 ← 3	185.31	2.384	-36.11	1.5
		1 ← 1	1/2	0	1 ← 3	185.54	-0.732	-36.05	1.5
		1 ← 1	1/2	-1	1 ← 3	185.79	-2.019	-36.21	1.5
6 ← 6	-1	5 ← 5	1/2	1	1 ← 3	140.57	-0.537	-35.03	1.5
		5 ← 5	1/2	0	1 ← 3	141.09	-0.766	-35.04	1.5
		5 ← 5	1/2	-1	1 ← 3	141.60	-2.698	-35.06	1.5
		5 ← 5	1/2		2 ← 3	645.21	-1.163	-22.26	1.5
		5 ← 5	-1/2		2 ← 3	643.95	-1.482	-22.27	1.5
		3 ← 3	1/2	1	1 ← 3	163.95	0.429	-35.54	1.5
		3 ← 3	1/2	0	1 ← 3	164.35	0.231	-35.55	1.5
		3 ← 3	1/2	-1	1 ← 3	164.82	1.680	-35.57	1.5
		3 ← 3	-1/2	1	1 ← 3	162.41	-1.289	-35.51	1.5
		3 ← 3	-1/2	0	1 ← 3	162.85	-0.070	-35.53	1.5
		3 ← 3	-1/2	-1	1 ← 3	163.22	-2.184	-35.55	1.5
		2 ← 2	-1/2	1	1 ← 3	177.10	2.215	-35.84	1.5
		2 ← 2	-1/2	0	1 ← 3	177.45	2.871	-35.91	1.5
		2 ← 2	-1/2	-1	1 ← 3	177.78	2.176	-35.98	1.5

TABLE 3—Continued

$N' \leftarrow N''$	Parity ^a	$M_J' \leftarrow M_J''$	$M_1(1^1\text{H})$	$M_1(1^4\text{N})$	eigenstate id. # ^b	B_0 (mT)	$\nu_L - \nu_c$ (MHz)	$\partial\nu/\partial B_0$ (MHz/mT)	Uncert. (MHz)
7 ← 7	1	6 ← 6	1/2		2 ← 3	701.18	-1.328	-22.80	1.5
		6 ← 6	-1/2		2 ← 3	699.92	-0.451	-22.81	1.5
1 ← 0	-1	0 ← 0	1/2		1 ← 1	1 458.16	-0.574	-25.68	3.0
		0 ← 0	-1/2		1 ← 1	1 456.72	-0.026	-25.67	3.0
		0 ← 1			1 ← 1	754.84 ^c	1.576	-45.03	4.0
<u>FIR Laser Frequency $\nu_L = 3\,696\,638.2$ MHz</u>									
7 ← 8	-1	8 ← 8	1/2	1	1 ← 1	671.93	7.332	23.86	0.0
		8 ← 8	1/2	0	1 ← 1	672.74	2.595	23.86	3.0
		8 ← 8	1/2	-1	1 ← 1	673.28	4.329	23.86	3.0
		8 ← 8	-1/2	1	1 ← 1	670.66	-4.444	23.88	3.0
		8 ← 8	-1/2	0	1 ← 1	671.23	-3.450	23.87	3.0
		8 ← 8	-1/2	-1	1 ← 1	671.93	-5.532	23.87	0.0
		-7 ← -7	1/2	1	2 ← 2	178.34	-1.203	-22.17	3.0
		-7 ← -7	1/2	0	2 ← 2	179.15	-0.452	-22.15	3.0
		-7 ← -7	1/2	-1	2 ← 2	179.99	0.904	-22.13	3.0
		-7 ← -7	-1/2	1	2 ← 2	176.54	0.535	-22.18	3.0
		-7 ← -7	-1/2	0	2 ← 2	177.30	0.184	-22.17	3.0
		-7 ← -7	-1/2	-1	2 ← 2	178.24	3.764	-22.15	3.0

TABLE 4
Details of the Microwave Data for $K_a = 0$ Included in the Least-Squares Fit (MHz)

$N' \leftarrow N''$	Parity ^a	$J' \leftarrow J''$	$F_1' \leftarrow F_1''$ ^b	$F' \leftarrow F''$	Frequency	obs. - calc.	Uncert.
1 ← 0	1 ← -1	0 ← 1	1/2 ← 3/2	3/2 ← 5/2	6 746.144	-0.001	0.005
	1 ← -1	0 ← 1	1/2 ← 3/2	3/2 ← 3/2	6 769.532	-0.002	0.005
	1 ← -1	0 ← 1	1/2 ← 3/2	1/2 ← 3/2	6 769.450	-0.002	0.005
	1 ← -1	0 ← 1	1/2 ← 3/2	1/2 ← 1/2	6 781.325	0.001	0.005
	1 ← -1	0 ← 1	1/2 ← 1/2	3/2 ← 3/2	6 686.830	-0.002	0.005
	1 ← -1	0 ← 1	1/2 ← 1/2	1/2 ← 3/2	6 686.762	0.012	0.005
	1 ← -1	0 ← 1	1/2 ← 1/2	3/2 ← 1/2	6 713.791	-0.006	0.005
	1 ← -1	2 ← 1	5/2 ← 3/2	7/2 ← 5/2	21 222.968	0.000	0.005
	1 ← -1	2 ← 1	5/2 ← 3/2	5/2 ← 5/2	21 199.230	-0.004	0.005
	1 ← -1	2 ← 1	3/2 ← 3/2	5/2 ← 5/2	21 279.424	0.002	0.005
	1 ← -1	2 ← 1	5/2 ← 3/2	5/2 ← 3/2	21 222.622	0.000	0.005
	1 ← -1	2 ← 1	5/2 ← 3/2	3/2 ← 3/2	21 208.130	-0.006	0.005
	1 ← -1	2 ← 1	3/2 ← 3/2	5/2 ← 3/2	21 302.812	0.001	0.005
	1 ← -1	2 ← 1	3/2 ← 3/2	3/2 ← 3/2	21 277.895	0.001	0.005
	1 ← -1	2 ← 1	3/2 ← 3/2	1/2 ← 3/2	21 264.580	0.001	0.005
	1 ← -1	2 ← 1	5/2 ← 3/2	3/2 ← 1/2	21 220.018	0.010	0.005
	1 ← -1	2 ← 1	3/2 ← 3/2	3/2 ← 1/2	21 289.765	-0.001	0.005
	1 ← -1	2 ← 1	3/2 ← 3/2	1/2 ← 1/2	21 276.450	-0.001	0.005
	1 ← -1	2 ← 1	3/2 ← 1/2	5/2 ← 3/2	21 220.108	-0.001	0.005
	1 ← -1	2 ← 1	3/2 ← 1/2	3/2 ← 3/2	21 195.191	-0.002	0.005
	1 ← -1	2 ← 1	3/2 ← 1/2	3/2 ← 1/2	21 222.160	0.002	0.005
	1 ← -1	2 ← 1	3/2 ← 1/2	1/2 ← 1/2	21 208.840	-0.002	0.005
5 ← 4	1 ← -1	4 ← 3			110 046.222	-0.062	0.050
6 ← 5	-1 ← 1	7 ← 6			131 762.851	0.031	0.050
	-1 ← 1	6 ← 5			131 833.305	-0.041	0.050
	-1 ← 1	5 ← 4			131 956.227	0.027	0.050

^a The parity is $-(-1)^{K_c}$ for a molecule in a level $N_{K_a K_c}$ of a $3A''$ state.^b Unlike Endo and Ohshima (11), we use the following coupling scheme in our fit: $J + I_H = F_1; F_1 + I_N = F$.

TABLE 5
Details of the Millimeter-Wave Data Included in the Least-Squares Fit (MHz)

$N' \leftarrow N''$	Parity ^a	$J' \leftarrow J''$	Frequency	obs. - calc.	Uncert.
$K_a = 0 \leftarrow 0$ ($v_5 = 0$)					
$7 \leftarrow 6$	$1 \leftarrow -1$	$8 \leftarrow 7$	153 746.186	-0.002	0.050
		$7 \leftarrow 6$	153 804.033	-0.020	0.050
		$6 \leftarrow 5$	153 894.083	0.019	0.050
$8 \leftarrow 7$	$-1 \leftarrow 1$	$9 \leftarrow 8$	175 724.839	-0.003	0.050
		$8 \leftarrow 7$	175 774.042	-0.018	0.050
		$7 \leftarrow 6$	175 844.436	0.004	0.050
$9 \leftarrow 8$	$1 \leftarrow -1$	$10 \leftarrow 9$	197 700.229	0.012	0.050
		$9 \leftarrow 8$	197 743.235	-0.031	0.050
		$8 \leftarrow 7$	197 800.949	-0.005	0.050
$11 \leftarrow 10$	$1 \leftarrow -1$	$12 \leftarrow 11$	241 643.862	0.024	0.050
		$11 \leftarrow 10$	241 678.864	-0.013	0.050
		$10 \leftarrow 9$	241 721.721	0.016	0.050
$12 \leftarrow 11$	$-1 \leftarrow 1$	$13 \leftarrow 12$	263 612.732	0.003	0.050
		$12 \leftarrow 11$	263 645.074	-0.008	0.050
		$11 \leftarrow 10$	263 683.362	0.028	0.050
$13 \leftarrow 12$	$1 \leftarrow -1$	$14 \leftarrow 13$	285 579.866	0.005	0.050
		$13 \leftarrow 12$	285 610.199	0.113	0.000
		$12 \leftarrow 11$	285 644.872	0.013	0.050
$15 \leftarrow 14$	$1 \leftarrow -1$	$16 \leftarrow 15$	329 508.958	-0.024	0.050
		$15 \leftarrow 14$	329 536.100	0.008	0.050
		$14 \leftarrow 13$	329 566.060	0.053	0.050
$16 \leftarrow 15$	$-1 \leftarrow 1$	$17 \leftarrow 16$	351 470.912	-0.032	0.050
		$16 \leftarrow 15$	351 496.907	0.013	0.050
		$15 \leftarrow 14$	351 525.028	-0.044	0.050
$17 \leftarrow 16$	$1 \leftarrow -1$	$18 \leftarrow 17$	373 431.074	-0.042	0.050
		$17 \leftarrow 16$	373 456.104	0.009	0.050
		$16 \leftarrow 15$	373 482.897	0.047	0.050
$18 \leftarrow 17$	$-1 \leftarrow 1$	$19 \leftarrow 18$	395 389.451	0.015	0.050
		$18 \leftarrow 17$	395 413.622	0.027	0.050
		$17 \leftarrow 16$	395 439.123	-0.046	0.050
$K_a = 1 \leftarrow 1$ ($v_5 = 1$)					
$5 \leftarrow 4$	$1 \leftarrow -1$	$6 \leftarrow 5$	109 458.916	0.268	0.000
		$4 \leftarrow 3$	109 475.559	0.182	0.000
	$-1 \leftarrow 1$	$6 \leftarrow 5$	109 880.665	0.194	0.000
		$5 \leftarrow 4$	110 506.607	-0.407	0.000
		$4 \leftarrow 3$	109 795.338	0.169	0.000
$7 \leftarrow 6$	$1 \leftarrow -1$	$8 \leftarrow 7$	153 435.756	-0.013	0.050
		$7 \leftarrow 6$	153 710.864	-0.007	0.050
		$6 \leftarrow 5$	153 530.900	-0.078	0.050
	$-1 \leftarrow 1$	$8 \leftarrow 7$	154 013.297	0.001	0.050
		$7 \leftarrow 6$	154 267.679	0.012	0.050
$8 \leftarrow 7$	$-1 \leftarrow 1$	$6 \leftarrow 5$	154 065.335	0.070	0.050
		$9 \leftarrow 8$	175 394.595	0.037	0.050
		$8 \leftarrow 7$	175 590.858	-0.042	0.050
	$1 \leftarrow -1$	$7 \leftarrow 6$	175 486.885	-0.030	0.050
		$9 \leftarrow 8$	176 051.160	-0.047	0.050
$9 \leftarrow 8$	$1 \leftarrow -1$	$8 \leftarrow 7$	176 232.257	-0.042	0.050
		$7 \leftarrow 6$	176 112.219	-0.066	0.050
		$10 \leftarrow 9$	197 344.217	0.005	0.050
	$-1 \leftarrow 1$	$9 \leftarrow 8$	197 491.533	-0.042	0.050
		$8 \leftarrow 7$	197 430.082	-0.036	0.050
$10 \leftarrow 9$	$-1 \leftarrow 1$	$10 \leftarrow 9$	198 080.413	-0.033	0.050
		$9 \leftarrow 8$	198 216.149	-0.016	0.050
		$8 \leftarrow 7$	198 142.697	-0.022	0.050

^a The parity is $-(-1)^{K_c}$ for a molecule in a level N_{KaKc} of a $^3A''$ state.

TABLE 5—Continued

$N' \leftarrow N''$	Parity a	$J' \leftarrow J''$	Frequency	obs. - calc.	Uncert.
11 ← 10	1 ← -1	12 ← 11	241 227.376	0.000	0.050
		11 ← 10	241 320.356	-0.026	0.050
	-1 ← 1	10 ← 9	241 300.410	0.008	0.050
		12 ← 11	242 123.578	-0.036	0.050
		11 ← 10	242 209.289	0.017	0.050
12 ← 11	-1 ← 1	10 ← 9	242 181.954	0.059	0.050
		13 ← 12	263 163.610	0.020	0.050
		12 ← 11	263 240.772	-0.044	0.050
	1 ← -1	11 ← 10	263 231.355	0.015	0.050
		13 ← 12	264 140.047	-0.032	0.050
		12 ← 11	264 211.316	0.017	0.050
13 ← 12	1 ← -1	11 ← 10	264 195.847	0.035	0.050
		14 ← 13	285 097.131	0.013	0.050
		13 ← 12	285 162.719	-0.043	0.050
		12 ← 11	285 160.417	0.019	0.050
	-1 ← 1	14 ← 13	286 153.921	-0.035	0.050
		13 ← 12	286 214.666	0.047	0.050
		12 ← 11	286 207.345	0.052	0.050
15 ← 14	1 ← -1	16 ← 15	328 957.339	0.042	0.050
		15 ← 14	329 007.612	0.092	0.050
		14 ← 13	329 013.742	0.122	0.050
	-1 ← 1	16 ← 15	330 175.029	0.030	0.050
16 ← 15	-1 ← 1	17 ← 16	350 884.230	-0.003	0.050
		16 ← 15	350 929.250	0.044	0.050
		15 ← 14	350 937.924	0.071	0.050
		17 ← 16	352 182.470	0.065	0.050
17 ← 16	1 ← -1	18 ← 17	372 809.086	-0.051	0.050
		17 ← 16	372 849.920	-0.012	0.050
		16 ← 15	372 860.463	0.009	0.050
		18 ← 17	374 187.913	0.128	0.050
	-1 ← 1	17 ← 16	374 225.892	-0.093	0.050
		16 ← 15	374 233.885	-0.058	0.050
		19 ← 18	394 731.966	-0.044	0.050
		17 ← 16	394 781.243	-0.109	0.050
18 ← 17	1 ← -1	19 ← 18	396 191.071	-0.054	0.050
		18 ← 17	396 226.374	0.067	0.050
		17 ← 16	396 235.937	-0.078	0.050
		19 ← 18	396 235.937	-0.078	0.050

HCCN and NCN, in particular, should be comparable because these molecules are isoelectronic. Indeed, the values for b_F and c are very similar. Using a value for the spin density on N in NCN of 0.5, the value of b_F for HCCN implies a spin density on the N atom of 0.55, broadly in line with the value of 0.34 obtained by Endo and Ohshima (11). The value $d = 1/2[(bb)_I - (cc)_I]$ for HCCN is very different from that for CCN. However, these two values are not really comparable since the interaction governed by this parameter arises solely from electrons in the π_g molecular orbital. There is only one such electron in CCN but there are two for HCCN; in the latter case the contributions from the two electrons almost cancel.

Another of the merits of the LMR experiment is that it provides quantitative information on the Zeeman parameters (or g -factors) of molecules. In the case of HCCN, we have been able to measure components of the electron spin $g_s^{\alpha\alpha}$ and the

rotational g -factor $g_r^{\alpha\alpha}$. A deviation from cylindrical symmetry was not detectable for either parameter. The electron spin g -factors were been determined previously by Bernheim *et al.* (3) for a randomly oriented sample in a glassy medium. Their values were $g_{\parallel} = g_s^{aa} = 2.073$ and $g_{\perp} = 1/2(g_s^{bb} + g_s^{cc}) = 2.013$, although they state that the former parameter was not well determined. The agreement with the present values is very poor. The discrepancy probably reflects the difficulty of interpreting ESR spectra of randomly oriented samples. The present values can also be compared with the expectations of Curl's relationship (42),

$$\Delta g \equiv g_s^{\alpha\alpha} - g_s = -\varepsilon_{\alpha\alpha}/(2B_{\alpha\alpha}), \quad [3]$$

where g_s is the isotropic g -factor for an electron spin. Taking g_s as 2.0020 (corrected for the relativistic increase in the mass

TABLE 6
Molecular Parameters for HCCN Determined in the Analysis of the $K_a = 1 - 0$ Band

Parameter	Value (MHz)	Value (cm^{-1})
A	3 875 550.09 (12) ^a	129.274 435 9 (40)
$1/2(B + C)$	10 986.408 76 (75)	0.366 467 150 (25)
$1/2(B - C)$	40.561 6 (12)	$0.135 299 1 (40) \times 10^{-2}$
D_N	$0.416 88 (16) \times 10^{-2}$	$0.139 056 (53) \times 10^{-6}$
D_{NK}	-2.116 08 (94)	$-0.705 85 (31) \times 10^{-4}$
d_1	$-0.576 (12) \times 10^{-4}$	$-0.192 1 (40) \times 10^{-8}$
H_{NK}	$-0.351 (20) \times 10^{-4}$	$-0.117 1 (67) \times 10^{-8}$
α	8 987.056 6 (38)	0.299 775 94 (13)
β	853.43 (28)	0.028 467 4 (93)
D_N^α	$0.363 (41) \times 10^{-2}$	$0.121 (14) \times 10^{-6}$
D_K^α	-267.32 (22)	$-0.891 68 (73) \times 10^{-2}$
H_{KN}^α	$-0.229 (53) \times 10^{-2}$	$-0.76 (18) \times 10^{-7}$
ϵ_{aa}	-8.47 (41)	$-0.283 (14) \times 10^{-3}$
$1/2(\epsilon_{bb} + \epsilon_{cc})$	-16.763 0 (21)	$-0.559 153 (70) \times 10^{-3}$
$1/2(\epsilon_{bb} - \epsilon_{cc})$	-0.554 (14)	$-0.184 8 (47) \times 10^{-4}$
$(D_{NK}^S + D_{KN}^S)$	0.671 (10)	$0.223 8 (33) \times 10^{-4}$
D_{NK}^S	-0.84 (11)	$-0.280 (37) \times 10^{-4}$
D_N^S	$0.38 (13) \times 10^{-4}$	$0.127 (43) \times 10^{-8}$
$a_F(\text{H})$	-41.722 7 (31)	$-0.139 172 (10) \times 10^{-2}$
$(aa)_I(\text{H})$	21.950 4 (81)	$0.732 19 (27) \times 10^{-3}$
$(bb)_I(\text{H})$	-5.84 (31)	$-0.195 (10) \times 10^{-3}$
$(cc)_I(\text{H})$	-16.11 ^b	$-0.537 4 \times 10^{-3b}$
$a_F(\text{N})$	11.573 8 (19)	$0.386 060 (63) \times 10^{-3}$
$(aa)_I(\text{N})$	-18.853 5 (50)	$-0.628 89 (17) \times 10^{-3}$
$(bb)_I(\text{N})$	7.46 (21)	$0.248 8 (70) \times 10^{-3}$
$(cc)_I(\text{N})$	11.39 ^b	$0.379 9 \times 10^{-3b}$
$(aa)_Q(\text{N})$	-1.948 1 (34)	$-0.649 8 (11) \times 10^{-4}$
$(bb)_Q(\text{N})$	0.974 ^c	0.325×10^{-4c}
g_{S}^{aa}		2.002 238 (42)
$1/2(g_{S}^{bb} + g_{S}^{cc})$		2.002 785 (34)
$1/2(g_{S}^{bb} - g_{S}^{cc})$		0.0 ^c
g_{r}^{aa}		-0.000 128 (60)
$1/2(g_{r}^{bb} + g_{r}^{cc})$		-0.000 050 (22)
$1/2(g_{r}^{bb} - g_{r}^{cc})$		0.0 ^c

^a Numbers in parentheses are one standard deviation and apply to the last quoted digits.

^b Not and independent value, determined from $(aa)_I + (bb)_I = -(cc)_I$.

^c Parameter constrained to this value in the fit (see text).

of the electron in a molecular environment), we obtain values for g_s^{aa} and $1/2(g_s^{bb} + g_s^{cc})$ of 2.0020 and 2.0028, respectively. The agreement with the present values in Table 6 is very good, increasing confidence in our analysis and interpretation.

The values for the rotational g -factors of HCCN are eminently reasonable. The electronic contribution to these g -factors can be estimated from the expression given by Brown and Sears (43)

$$g_r^{\alpha\alpha}(\text{el}) = -|\epsilon_{\alpha\alpha}|/\zeta, \quad [4]$$

where ζ is the effective spin-orbit coupling constant for the open-shell electrons. Using the spin densities of 0.34 on N and

0.66 on C₁ from Endo and Ohshima (11), we estimate ζ to be 43.1 cm^{-1} in HCCN. This gives $g_r^{aa}(\text{el}) = -0.66 \times 10^{-5}$ and $1/2(g_r^{bb} + g_r^{cc})(\text{el}) = -0.130 \times 10^{-4}$. The corresponding experimental values (see Table 6) are somewhat larger in magnitude, which is surprising because the nuclear contribution to these rotational g -factors is expected to be positive. The formula in Eq. [4] is unlikely to be very reliable for g_r^{aa} because this g -factor will also have a contribution from vibrational angular momentum in the $v_5 = 1$ level.

The accurate characterization of the $K_a = 1 \leftarrow 0$ transition frequencies for HCCN provides a distinctive and sensitive

TABLE 7
Molecular Parameters for HCCN, Expressed in the Linear Molecule Notation

Parameter	Value (MHz)	Value (cm ⁻¹)	Previous Value	Ref.
ν_5	3 864 563.68 (12) ^a	128.907 968 7 (40)	128.907 (2) ^b	(15)
B_0	10 986.408 76 (75)	0.366 467 150 (25)	10 986.408 7 (4)	(13)
D_0	0.416 88 (16) $\times 10^{-2}$	0.139 056 (53) $\times 10^{-6}$	0.416 87 (9) $\times 10^{-2}$	(13)
γ_0	-16.763 0 (21)	-0.559 153 (70) $\times 10^{-3}$	-16.737 (8)	(13)
γ_{D0}	0.38 (13) $\times 10^{-4}$	0.127 (43) $\times 10^{-8}$	-0.108 (38) $\times 10^{-3}$	(11)
λ_0	13 480.584 9 (57)	0.449 663 91 (19)	13 480.575 (11)	(11)
λ_{D0}	0.544 (62) $\times 10^{-2}$	0.182 (21) $\times 10^{-6}$	0.55 (3) $\times 10^{-2}$	(13)
B_1	10 988.5248 (12)	0.366 537 735 (40)	10 988.5251 (3)	(13)
D_1	0.420 39 (26) $\times 10^{-2}$	0.140 227 (87) $\times 10^{-6}$	0.420 42 (6) $\times 10^{-2}$	(13)
γ_1	-16.092 (10)	-0.536 77 (34) $\times 10^{-3}$	-16.119 (3)	(13)
λ_1	13 079.60 (33)	0.436 289 (11)	13 062.6 (3)	(13)
λ_{D1}	0.201 (100) $\times 10^{-2}$	0.670 (334) $\times 10^{-7}$	0.35 (3) $\times 10^{-2}$	(13)
o_G	-853.43 (28)	-0.284 674 (93) $\times 10^{-1}$	-853.0 (3) ^c	(13)
p_G	-0.554 (14)	-0.184 8 (47) $\times 10^{-4}$	-0.579 (8) ^c	(13)
q_G	-40.561 6 (12)	-0.135 299 1 (40) $\times 10^{-2}$	-40.560 7 (6) ^c	(13)
q_{GD}	0.115 2 (24) $\times 10^{-3}$	0.384 3 (80) $\times 10^{-8}$	0.113 (1) $\times 10^{-3}$ ^c	(13)
b_F (¹ H)	-41.722 7 (31)	-0.139 172 (10) $\times 10^{-2}$	-41.723 (9)	(11)
c (¹ H)	32.926 (12)	0.109 828 (41) $\times 10^{-2}$	32.91 (7)	(11)
b_F (¹⁴ N)	11.573 8 (19)	0.386 060 (63) $\times 10^{-3}$	11.573 (6)	(11)
c (¹⁴ N)	-28.280 3 (75)	-0.943 33 (25) $\times 10^{-3}$	-28.291 (43)	(11)
eQq_0 (¹⁴ N)	-3.896 2 (68)	-0.129 96 (23) $\times 10^{-3}$	-3.897 (20)	(11)

^a The numbers in parentheses represent one standard deviations of the least-squares fit, in units of the last quoted decimal place.

^b The values for the parameters obtained by other workers are given in MHz, with the exception of that for ν_5 which is given in cm⁻¹.

^c McCarthy *et al.* (13) determined values for the lambda-type doubling parameters o , p and q which have the opposite signs.

way of detecting the molecule in remote sources such as the circumstellar shells or the interstellar medium. To aid this process, we have calculated the zero-field frequencies of the first few lines in the P , Q , and R branches from the parameters in Table 6. For the sake of simplicity, nuclear hyperfine structure has not been included. The results are given in Table 9.

The degree of quasi-linearity of HCCN cannot be assessed from the $K_a = 1 \leftarrow 0$ data set by itself. As we have seen, a linear and a bent model of the molecule can fit it equally well.

For this reason, it is desirable to obtain information on the location of the $K_a = 2$ levels (which correspond to the $\nu_5 = 2$, $l_5 = 2$ levels in the linear designation) and also of higher levels. According to the intensity measurements of McCarthy *et al.* (13), if we scale the levels by the same ratio we have determined for the $\nu_5 = 1$ ($129 \text{ cm}^{-1}/145 \text{ cm}^{-1} = 0.89$) then the $K_a = 2 \leftarrow 1$ subband is expected to occur between 150 and 190 cm^{-1} (4.50 and 5.70 THz). We are currently searching for HCCN signals in this general region.

TABLE 8
¹⁴N Hyperfine Parameters (in MHz) for HCCN and Related Species in Their Ground Electronic States

Parameter	HCCN ^a	NCN ^b	CCN ^c
b_F	11.573 8 (19)	14.1	9.13 (25)
c	-28.280 3 (75)	-25.9	-30.92 (75)
d	-1.97 (10)		46.767 38 (53)
eQq_0	-3.896 2 (68)		-4.822 1 (14)

^a This work.

^b Ref. (42)

^c Ref. (37)

TABLE 9
Zero-Field Frequencies for the $K_a = 1 \leftarrow 0$ ($v_5 = 1 \leftarrow 0$) Transition Calculated Using the
Molecular Parameters Determined in This Work^a

$N' \leftarrow N''$	$J' \leftarrow J''$	Parity ^b	Frequency (MHz)	Line strength
1 ← 2	2 ← 3	1 ← -1	3 823 188.943	1427
	1 ← 2		3 803 853.846	308
	0 ← 1		3 834 702.197	471
2 ← 3	3 ← 4	-1 ← 1	3 799 832.766	2304
	2 ← 3		3 794 200.931	1269
	1 ← 2		3 802 662.952	1052
3 ← 4	4 ← 5	1 ← -1	3 777 236.107	3115
	3 ← 4		3 774 360.840	2184
	2 ← 3		3 777 917.620	1793
4 ← 5	5 ← 6	-1 ← 1	3 754 858.339	3862
	4 ← 5		3 753 141.888	2997
	3 ← 4		3 754 987.585	2518
5 ← 6	6 ← 7	1 ← -1	3 732 554.171	4543
	5 ← 6		3 731 439.124	3726
	4 ← 5		3 732 506.748	3202
6 ← 7	7 ← 8	-1 ← 1	3 710 269.589	5156
	6 ← 7		3 709 508.038	4378
	5 ← 6		3 710 157.698	3834
7 ← 8	8 ← 9	1 ← -1	3 687 980.517	5698
	7 ← 8		3 687 444.850	4955
	6 ← 7		3 687 844.241	4405
8 ← 9	9 ← 10	-1 ← 1	3 665 674.859	6167
	8 ← 9		3 665 292.485	5458
	7 ← 8		3 665 530.200	4912
9 ← 10	10 ← 11	1 ← -1	3 643 345.996	6562
	9 ← 10		3 643 072.488	5887
	8 ← 9		3 643 199.728	5352
1 ← 1	2 ← 2	-1 ← 1	3 867 087.615	3713
	1 ← 1		3 847 441.084	330
2 ← 2	3 ← 3	1 ← -1	3 866 049.923	5683
	2 ← 2		3 859 772.259	2972
3 ← 3	1 ← 1	-1 ← 1	3 870 843.454	1638
	4 ← 4		3 865 761.177	7486
	3 ← 3		3 862 030.579	5096
4 ← 4	2 ← 2	1 ← -1	3 867 540.350	3648
	5 ← 5		3 865 734.444	9175
	4 ← 4		3 863 053.113	6971
5 ← 5	3 ← 3	-1 ← 1	3 866 605.675	5516
	6 ← 6		3 865 843.020	10757
	5 ← 5		3 863 698.091	8681
6 ← 6	4 ← 4	1 ← -1	3 866 354.548	7230
	7 ← 7		3 866 040.916	12226
	6 ← 6		3 864 207.197	10250
7 ← 7	5 ← 5	-1 ← 1	3 866 378.936	8811
	8 ← 8		3 866 308.023	13574
	7 ← 7		3 864 670.812	11684
8 ← 8	6 ← 6	1 ← -1	3 866 550.135	10266
	9 ← 9		3 866 634.386	14793
	8 ← 8		3 865 129.053	12981
9 ← 9	7 ← 7	-1 ← 1	3 866 817.988	11591
	10 ← 10		3 867 014.614	15875
	9 ← 9		3 865 601.952	14137
10 ← 10	8 ← 8	1 ← -1	3 867 159.754	12783
	11 ← 11		3 867 445.576	16814
	10 ← 10		3 866 100.423	15150
	9 ← 9		3 867 563.910	13835

^a Hyperfine structure is ignored and only $\Delta J = \Delta N$ transitions are given, except for $N = 1 \leftarrow 0$.

^b The parity is $(-1)^{K_c}$ for a molecule in a level $N_{K_a K_c}$ of a $^3A''$ state.

TABLE 9—Continued

$N' \leftarrow N''$	$J' \leftarrow J''$	Parity ^b	Frequency (MHz)	Line strength
1 ← 0	2 ← 1	1 ← -1	3 888 035.329	2894
	1 ← 1		3 881 482.316	2068
	0 ← 1		3 897 096.362	417
2 ← 1	3 ← 2	-1 ← 1	3 909 190.657	3767
	2 ← 1		3 904 064.471	2413
	1 ← 0		3 924 987.193	458
3 ← 2	4 ← 3	-1 ← 1	3 930 737.065	4655
	3 ← 2		3 928 169.095	3410
	2 ← 1		3 932 797.702	1901
4 ← 3	5 ← 4	-1 ← 1	3 952 397.503	5538
	4 ← 3		3 950 894.158	4356
	3 ← 2		3 953 245.350	3096
5 ← 4	6 ← 5	1 ← -1	3 974 088.887	6403
	5 ← 4		3 973 134.510	5267
	4 ← 3		3 974 509.231	4132
6 ← 5	7 ← 6	-1 ← 1	3 995 778.597	7238
	6 ← 5		3 995 145.437	6138
	5 ← 4		3 996 007.961	5079
7 ← 6	8 ← 7	1 ← -1	4 017 451.548	8031
	7 ← 6		4 017 022.963	6965
	6 ← 5		4 017 582.736	5960
8 ← 7	9 ← 8	-1 ← 1	4 039 099.919	8775
	8 ← 7		4 038 809.811	7741
	7 ← 6		4 039 175.586	6779
9 ← 8	10 ← 9	1 ← -1	4 060 719.289	9462
	9 ← 8		4 060 527.326	8459
	8 ← 7		4 060 761.272	7534
10 ← 9	11 ← 10	-1 ← 1	4 082 306.982	10084
	10 ← 9		4 082 187.120	9112
	9 ← 8		4 082 327.372	8223
11 ← 10	12 ← 11	1 ← -1	4 103 861.283	10635
	11 ← 10		4 103 795.930	9696
	10 ← 9		4 103 867.184	8841

REFERENCES

- R. A. Bernheim, R. J. Kempf, P. W. Humer, and P. S. Skell, *J. Chem. Phys.* **41**, 1156–1157 (1964).
- R. A. Bernheim, R. J. Kempf, J. V. Gramas, and P. S. Skell, *J. Chem. Phys.* **43**, 196–200 (1965).
- R. A. Bernheim, R. J. Kempf, and E. F. Reichenbecher, *J. Magn. Res.* **3**, 5–9 (1970).
- E. Wasserman, W. A. Yager, and V. J. Kuck, *Chem. Phys. Lett.* **7**, 409–413 (1970).
- A. J. Merer and D. N. Travis, *Can. J. Phys.* **43**, 1795–1818 (1965).
- A. J. Merer and D. N. Travis, *Can. J. Phys.* **44**, 353–372 (1966).
- A. Dendramis and G. F. Leroi, *J. Chem. Phys.* **66**, 4334–4340 (1977).
- S. Saito, Y. Endo, and E. Hirota, *J. Chem. Phys.* **80**, 1427–1430 (1984).
- F. X. Brown, S. Saito, and S. Yamamoto, *J. Mol. Spectrosc.* **143**, 203–208 (1990).
- C. L. Morter, S. K. Farhat, and R. F. Curl, *Chem. Phys. Lett.* **207**, 153–158 (1993).
- Y. Endo and Y. Ohshima, *J. Chem. Phys.* **98**, 6618–6623 (1993).
- C. E. Miller, W. C. Eckhoff, and R. F. Curl, *J. Mol. Struct.* **352/353**, 435–446 (1995).
- M. C. McCarthy, C. A. Gottlieb, A. L. Cooksy, and P. Thaddeus, *J. Chem. Phys.* **103**, 7779–7787 (1995).
- F. Sun, A. Kosterev, G. Scott, V. Litosh, and R. F. Curl, *J. Chem. Phys.* **109**, 8851–8856 (1998).
- J.-X. Han, P. Y. Hung, J. DeSain, W. E. Jones, and R. F. Curl, *J. Mol. Spectrosc.* **198**, 421–428 (1999).
- N. Goldberg, A. Fiedler, and H. Schwarz, *J. Phys. Chem.* **99**, 15,327–15,334 (1995).
- R. Hoffman, G. D. Zeiss, and G. V. VanDine, *J. Am. Chem. Soc.* **90**, 1485–1493 (1968).
- J. F. Harrison, A. Dendramis, and G. F. Leroi, *J. Am. Chem. Soc.* **100**, 4352–4356 (1978).
- N. C. Baird and K. F. Taylor, *J. Am. Chem. Soc.* **100**, 1333–1338 (1978).
- M. E. Zandler, J. D. Goddard, and H. F. Schaefer III, *J. Am. Chem. Soc.* **101**, 1072–1076 (1979).
- P. H. Mueller, N. G. Rondan, K. N. Houk, J. F. Harrison, D. Hooper, B. H. Willen, and J. F. Liebman, *J. Am. Chem. Soc.* **103**, 5049–5052 (1981).
- K. S. Kim, H. F. Schaefer III, L. Radom, J. A. Pople, and J. S. Binkley, *J. Am. Chem. Soc.* **105**, 4148–4154 (1983).
- J. E. Rice and H. F. Schaefer III, *J. Chem. Phys.* **86**, 7051–7053 (1965).
- P. A. Malmquist, R. Lindh, B. O. Roos, and S. Ross, *Theor. Chim. Acta* **73**, 155–171 (1988).
- E. T. Seidl and H. F. Schaefer III, *J. Chem. Phys.* **96**, 4449–4452 (1992).
- C. B. Kellogg, J. M. Galbraith, J. E. Fowler, and H. F. Schaefer III, *J. Chem. Phys.* **101**, 430–435 (1994).
- J. S. Francisco, *Chem. Phys. Lett.* **230**, 372–376 (1994).
- M. Guélin and J. Chernicharo, *Astron. Astrophys.* **244**, L21–L24 (1991).

29. W. E. Jones, F. Sun, R. F. Curl, M. D. Allen, K. M. Evenson, and J. M. Brown, *Can. J. Phys.* **79**, 389–408 (2001).
30. See AIP document No. PAPS 103-7779-15 for 15 pages of tables. Order by PAPS number and journal reference from American Institute of Physics, Physics Auxiliary Publication Service, Carolyn Gehlbach, 500 Sunnyside Blvd., Woodbury, NY 11797–2999. Fax: (516) 576-2223. E-mail: janis@aip.org.
31. R. J. Saykally, K. G. Lubic, A. Scalabrin, and K. M. Evenson, *J. Chem. Phys.* **77**, 58–67 (1982).
32. J. M. Brown, L. R. Zink, and K. M. Evenson, *Phys. Rev. A* **57**, 2507–2510 (1998).
33. S. A. Beaton and J. M. Brown, *J. Mol. Spectrosc.* **183**, 347–359 (1997).
34. T. J. Sears, P. R. Bunker, A. R. W. McKellar, K. M. Evenson, D. A. Jennings, and J. M. Brown, *J. Chem. Phys.* **77**, 5348–5362 (1982).
35. T. J. Sears, *Comp. Phys. Rep.* **2**, 1–32 (1984).
36. J. K. G. Watson, in “Vibrational Spectra and Structure” (J. R. Durig, Ed.), Vol. 6, Chap. 1. (Elsevier, New York, 1977).
37. D. R. Lide, Ed., “Handbook of Chemistry and Physics,” 74th ed., pp. 11–37. CRC Press, Ann Arbor, MI, 1993–1994.
38. M. D. Allen, K. M. Evenson, D. A. Gillett, and J. M. Brown, *J. Mol. Spectrosc.* **201**, 18–29 (2000).
39. C. A. Schmuttenmaer, R. C. Cohen, N. Pugliano, J. R. Heath, A. L. Cooksy, K. L. Busarow and R. J. Saykally, *Science* **249**, 897–900 (1990).
40. H. Körsgen, K. M. Evenson, and J. M. Brown, *J. Chem. Phys.* **107**, 1025–1027 (1997).
41. H. U. Suter, M.-B. Huang, and B. Engels, *J. Chem. Phys.* **101**, 7686–7691 (1988).
42. R. F. Curl, *Mol. Phys.* **9**, 585–597 (1965).
43. J. M. Brown and T. J. Sears, *J. Mol. Spectrosc.* **75**, 111–133 (1979).